Fuel 371 (2024) 131867

Contents lists available at ScienceDirect

Fuel

journal homepage: www.elsevier.com/locate/fuel

Full length article

Comparative analysis of pyrolysis models including SFOR, CRECK, and Bio-CPD to predict reaction kinetics and products from extracted biomass components

Stefan Pielsticker [a,*], Paulo Debiagi [b], Francesca Cerciello [c], Christian Hasse [d], Reinhold Kneer [a]

[a] Institute of Heat and Mass Transfer (WSA), RWTH Aachen University, Augustinerbach 6, 52056 Aachen, Germany
[b] China Beacons Institute, University of Nottingham Ningbo China, No. 211, Xingguang Road, Yinzhou District, Ningbo, China
[c] Laboratory of Industrial Chemistry, Ruhr-Universität Bochum, Universitätsstraße 150, 44780 Bochum, Germany
[d] Institute for Simulation of Reactive Thermo-Fluid Systems (STFS), Technische Universität Darmstadt, Otto-Berndt-Str. 2, 64287 Darmstadt, Germany

ARTICLE INFO

Dataset link: https://doi.org/10.18154/RWTH-2024-02457, https://doi.org/10.18154/RWTH-2021-05544

Keywords:
Biomass pyrolysis
Kinetic modeling
Fluidized bed reactor
Thermogravimetric analysis
Secondary gas-phase reactions

ABSTRACT

Biomass pyrolysis is typically modeled based on the three reference components cellulose, hemicellulose, and lignin. Most models rely on an individual decomposition of the materials and a linear superposition of the individual component products weighted by the present mass fractions. Models of varying complexity exist for the mathematical description of the pyrolysis process, ranging from the simplest single first-order (SFOR) model and the multi-step CRECK model to the chemical percolation devolatilization (CPD) model representing the molecular network of the solid. The models differ not only in their complexity but also in the used data for initial parameter calibration — thermogravimetric analysis (TGA) data for the CRECK model and mainly entrained flow, fluidized bed, or wire mesh reactor data for the Bio-CPD model. Within the present study, the predictive performance of these three models is compared with regard to the time-dependent total volatile release and the final volatile yield when applying two different thermal boundary conditions: low heating rate in a TGA and flash pyrolysis conditions realized with a small-scale fluidized bed reactor (FBR). The models are compared with one other and with experimental data on extracted, separately pyrolyzed biomass components to examine under which conditions reliable predictions can be made and when the trustability is limited. For the TGA data, the CRECK model has the closest proximity to the experimental measurements, also resolving most of the individual reactions, while the SFOR model can resolve only one globally dominating reaction, and the Bio-CPD model strongly overpredicts the reactivity of the biomass components during the slow heat-up. Under flash pyrolysis conditions in the FBR, by contrast, the Bio-CPD model predictions are closest to the experimental results when it comes to predicting the total volatile release rate. However, examining the integrally released yields, the CRECK model is closer to the experiments. Regarding the tar and light gas distribution, all models strongly overpredict tar from primary pyrolysis compared to the experimental results, indicating the presence of secondary gas-phase reactions in the FBR. Although different secondary gas-phase reaction models are used, the tar yield is significantly overestimated by the models compared to the experimental data.

1. Introduction

Biomass is crucial for mitigating human-caused greenhouse gas emissions by transitioning from fossil towards renewable energy sources. Biomass pyrolysis, the treatment of solid biogenic material in an oxygen-free environment, raises the value of agricultural and organic waste by transforming it into valuable products such as biochar and bio-oil. At the same time, a sustainable carbon circular economy can be established while anthropogenic CO_2 emissions are reduced.

Modeling of pyrolysis is a challenging problem as pyrolysis is known to be a multi-component, multi-phase, and multi-scale process [1]. Biomass is typically split into three main components: cellulose, hemicellulose, and lignin. Additionally, depending on the biomass, extractives such as phenols, tannins, resins, waxes, lipids, and proteins account for a minor fraction in the mass composition. Most common modeling approaches assume that each component has its own independent composition during the pyrolysis process and describe the

* Corresponding author.
E-mail address: pielsticker@wsa.rwth-aachen.de (S. Pielsticker).

https://doi.org/10.1016/j.fuel.2024.131867
Received 10 November 2023; Received in revised form 6 April 2024; Accepted 10 May 2024
Available online 24 May 2024

Nomenclature

Greek

α	Convective heat transfer coefficient $\mathrm{W\,m^{-2}\,K^{-1}}$
Γ	Eulerian gamma function –
ε	Emissivity –
μ	Mean value
ρ	Density $\mathrm{kg\,m^{-3}}$
σ	Coordination number –
σ	Standard deviation
σ	Stefan–Boltzmann constant $\mathrm{W\,m^{-2}\,K^{-4}}$
φ	Volume fraction –

Latin

A	Pre-exponential factor $1/\mathrm{s}$
B	Boolean function –
Bi	Biot number –
c	Specific heat capacity $\mathrm{J\,kg^{-1}\,K^{-1}}$
d	Diameter m
E_a	Activation energy $\mathrm{J\,mol^{-1}}$
H	Height m
h	Specific enthalpy $\mathrm{J\,kg^{-1}}$
L	Length m
M	Molar mass $\mathrm{kg\,mol^{-1}}$
m	Molecular weight u
m	Mass kg
$\dot{m}$	Mass flow $\mathrm{kg\,s^{-1}}$
N	Number –
P	Probability –
Py	Pyrolysis number –
R	Universal gas constant $\mathrm{J\,mol^{-1}\,K^{-1}}$
r	Reaction rate $1/\mathrm{s}$
r^*	Reaction rate ratio –
S	Surface area $\mathrm{m^2}$
T	Temperature K
t	Time s
$\dot{V}$	Volume flow $\mathrm{m^3\,s^{-1}}$
X	Bridge fraction –
y	Yield –

Subscripts

∞	Completed pyrolysis process
0	Initial value
10	10%
50	50%
90	90%
a	Ash
act	Activated
ar	Aromatic part
bro	Broken
char	Char
cl	Cluster
conf	Configuration
cross	Cross-linking
exp	Experimental
ext	External from particle
FB	Fluidized bed
FP	Fedd pipe
frag	Fragment
g	Gas
GPR	Gas-phase reaction
i	ith component
int	Intact
lab	Labile
LG	Light gas
N_2	Nitrogen
n	Norm conditions
p	Particle
PT	Percolation theory
reac	Reaction
s	Solid material
SC	Side chain
stab	Stable
tar	Tar
tot	Total
v	Volatiles

Superscripts

”	Gaseous phase
’	Liquid phase

Abbreviations

CFD	Computational fluid dynamics
CPD	Chemical percolation devolatilization
CRECK	Chemical reaction engineering and chemical kinetics
FBR	Fluidized bed reactor
FTIR	Fourier-transform infrared (spectrometer)
IR	Infrared
PT	Percolation theory
SFOR	Single first-order reaction
TGA	Thermogravimetric analysis
VLE	Vapor–liquid equilibrium

overall product by means of linear superposition. Although the mineral components in the biomass influence the product spectrum and the reaction rates (typically the tar yield is reduced at the expense of the char and light gas yields), this is only considered in some models, e.g., by Ranzi et al. [2], but still neglected in most current models [3]. Compared to natural biomass, the extracted components – especially hemicellulose – may even show higher concentrations of catalysts originating from the extraction process [4]. Hameed et al. [5] and Vikram et al. [3] describe the spectrum of prevailing biomass pyrolysis models, which can be grouped into three categories: kinetic models, network models, and mechanistic models. Mechanistic models can help understanding decomposition behavior at a molecular level but exceed available computational resources when it comes to the full-scale simulation of biomass pyrolysis processes [5].

Network models attempt to represent the molecular structure at an abstract level by interpreting biomass as a network with connections of variable stability without resolving any elemental reaction. This category is most suitable for understanding the effects of particle heat-up, particle-internal transport phenomena, and structural changes such as fragmentation. Notable examples of the network models commonly employed for pyrolysis include the chemical percolation devolatilization model (CPD) [6–8], the functional group depolymerization vaporization crosslinking model (FG-DVC) [9–11], and the flash distillation

chain statistics model (FLASHCHAIN) [12–15]. In addition to the consideration of purely chemical processes, for the (Bio-)CPD model, various extensions have also attempted to take into account the effects of particle-internal heat and mass transfer [16,17], the feedback of cross-linking on the network structure [18], or the catalytic activity of mineral components [19].

Purely kinetic models describe the conversion process as a systematic combination of parallel and sequential reactions. The discretization of educts and products can involve one lumped component, e.g., in the single first-order model (SFOR) [20] or multiple individual reaction species, e.g., in the chemical reaction engineering and chemical kinetics model (CRECK). Purely kinetic models have the advantage of being easily coupled with simulations of the computational fluid dynamics for full-scale reactors [5]. In addition to primary decomposition, secondary reactions in the gas phase or between volatiles and char [3] determine product quantity and composition. Charring reactions are expected to be mostly important for larger particles, where particle-internal volatiles (metaplast) have longer contact times with the char matrix [21]. The level of detail of the available secondary gas-phase reaction models ranges from simple one-step models for tar cracking to detailed gas-phase kinetic models with multiple reaction pathways and species [22].

Most primary pyrolysis models were initially developed based on pyrolysis experiments with coal and have been subsequently adapted for biogenic solids. During the calibration and validation procedure, experimental data from different laboratory setups and different fuels (biomass vs. extracted components) were used. While the CRECK model is mainly validated against experimental data from thermogravimetric analyses (TGA) performed at relatively low heating rates (3–80 $K\,min^{-1}$) [2,23,24], the biomass version of the CPD model is mainly validated against experiments with high heating rates (10^3–10^5 $K\,s^{-1}$). In most calibration scenarios, integrally released fractions of light gas, tar and the remaining char [25–30] were used to compare the experiments and the model's predictions [31–35]. The usage of time-dependent data on the pyrolysis products released from biomass under flash pyrolysis conditions is only documented by Lewis and Fletcher [34] and Rabaçal et al. [35]. In both studies, mainly the final phase is captured, while the main conversion is only reflected by one data point. This makes it impossible to judge whether the model correctly predicts the relevant time scales. For extracted and separated biomass components, to the author's best knowledge, no comprehensive evaluation on the performance of flash pyrolysis modeling using time-dependent data can be found in the literature.

In addition to the comparison with experimental data, the model's performances were also compared with one other. Using coal as a fuel, the study by Maffei et al. [36] compared the CPD model against the CRECK model, while Richards and Fletcher [37] compared the CPD model with other simple kinetic models. The comparison of the final volatile yields for four different coals performed by Maffei et al. [36] showed that the CRECK model was more sensitive with respect to the origin of the coal, but no clear trend was found that showed, which model better predicted the experimental results. In the study by Richards and Fletcher [37], the aim was to evaluate how simple kinetic models (e.g., the SFOR model) can represent the CPD predictions without having any experimental reference data. The SFOR model could not represent any effect of the heating rate and strongly overpredicted the total volatile release rate compared to the CPD predictions. For biomass, Xing et al. [38] recently compared the CRECK and Bio-CPD (version found in Fletcher et al. [33]) models with regard to TGA experiments on various biomass samples. The Bio-CPD model did not accurately predict the pyrolysis process and overestimated the final volatile yields for all samples. The study by Rabaçal et al. [35] is the only one that compares the CRECK and Bio-CPD models for biomass pyrolysis at high heating rates against experimental reference data from a drop-tube reactor operated between 973 and 1673 K [28,29]. Both models underpredicted the total volatile release compared to the experimental findings at all temperatures for both the biomasses investigated, with the CRECK model producing even lower total volatile yields than the Bio-CPD model. While the CRECK model was able to correctly reflect the temperature trends, the Bio-CPD model did not show any sensitivity with regard to the final yield to the temperature. Regarding the volatile composition, the Bio-CPD model predicts high tar yields around 70 to 80% and low light gas yields while the CRECK model gives tar yields between 40 to 70%. As tar cracking is taken into account by the model developed by Vizzini et al. [32], the tar yields indicated using CRECK and Bio-CPD approach converge but are still significantly higher than in the experimental data at levels around 10 to 30%.

The goal of this study is to comprehensively compare the simple (SFOR) and complex (CRECK) kinetic models on the one hand with the Bio-CPD network model on the other hand. To minimize the effects of interactions between the components, experimental reference data on extracted and separately pyrolyzed samples are used. To simultaneously achieve the high heating rates of flash pyrolysis and investigate the entire pyrolysis process, data from a fluidized bed reactor with coupled *ex-situ* and time-resolved gas analysis is utilized [39]. Due to the particles' unlimited residence time inside the fluidized bed, these data make it possible to analyze time-dependent release rates and the integrally released volatile reaction products. To complete the model comparison, the relevance of secondary pyrolysis reactions in the fluidized bed reactor is evaluated and the models' performance at low particle heating rates is investigated using thermogravimetric analyses. Comparing the model performance also at other than the calibration conditions is important as both models are also widely used for the opposite boundary conditions: e.g., the CRECK model for high heating rates [40–44] or the Bio-CPD for low heating rates [38]. However, the aim of the study is not to select the best overall model but to raise awareness of the conditions under which model predictions can be trusted and when model predictions should be viewed carefully.

2. Experimental reference data

In a previous study entitled *"Flash Pyrolysis Kinetics of Extracted Lignocellulosic Biomass Components"* [39], the pyrolysis kinetics of cellulose, hemicellulose, and lignin were investigated individually using two different experimental setups: a thermogravimetric analyzer and a small-scale fluidized bed reactor. To minimize the impact of intra-particle transport limitations and moisture evaporation, pre-dried and pulverized fuel samples were used with mesh sizes of 90–125 μm (cellulose and lignin) and 60–90 μm (hemicellulose). Important fuel characteristics derived via ultimate, proximate, and microscopic particle size analysis are given in Table 1.

Thermogravimetric analyses (TGA) using a TGA8000 from Perkin Elmer Inc. were used to determine the pyrolysis kinetics of lignocellulosic components at low temperatures and low heating rates. The sample (0.8–1.2 mg in an alumina crucible) was heated in N_2 (volume flow 50 $ml\,min^{-1}$, purity > 99.996%) from 303 K to 1173 K with a constant heating rate of 5 $K\,min^{-1}$ [39].

2.1. Fluidized bed reactor

Pyrolysis kinetics are determined in a fluidized bed reactor (FBR) – as illustrated in Fig. 1 – by analyzing the released volatiles with an *ex-situ* Fourier-transform infrared spectrometer. The FBR setup offers a combination of high particle heating rates, up to around 10^4 $K\,s^{-1}$, and moderate temperatures ranging from T_b = 623–1073 K. The unlimited residence time of the particles further enables the entire conversion process to be captured.

The system consists of three main parts: a controlled gas supply, the reaction zone in the fluidized bed, and the *ex-situ* FTIR spectrometer for gas analysis. The gas supply and the electrically heated furnace

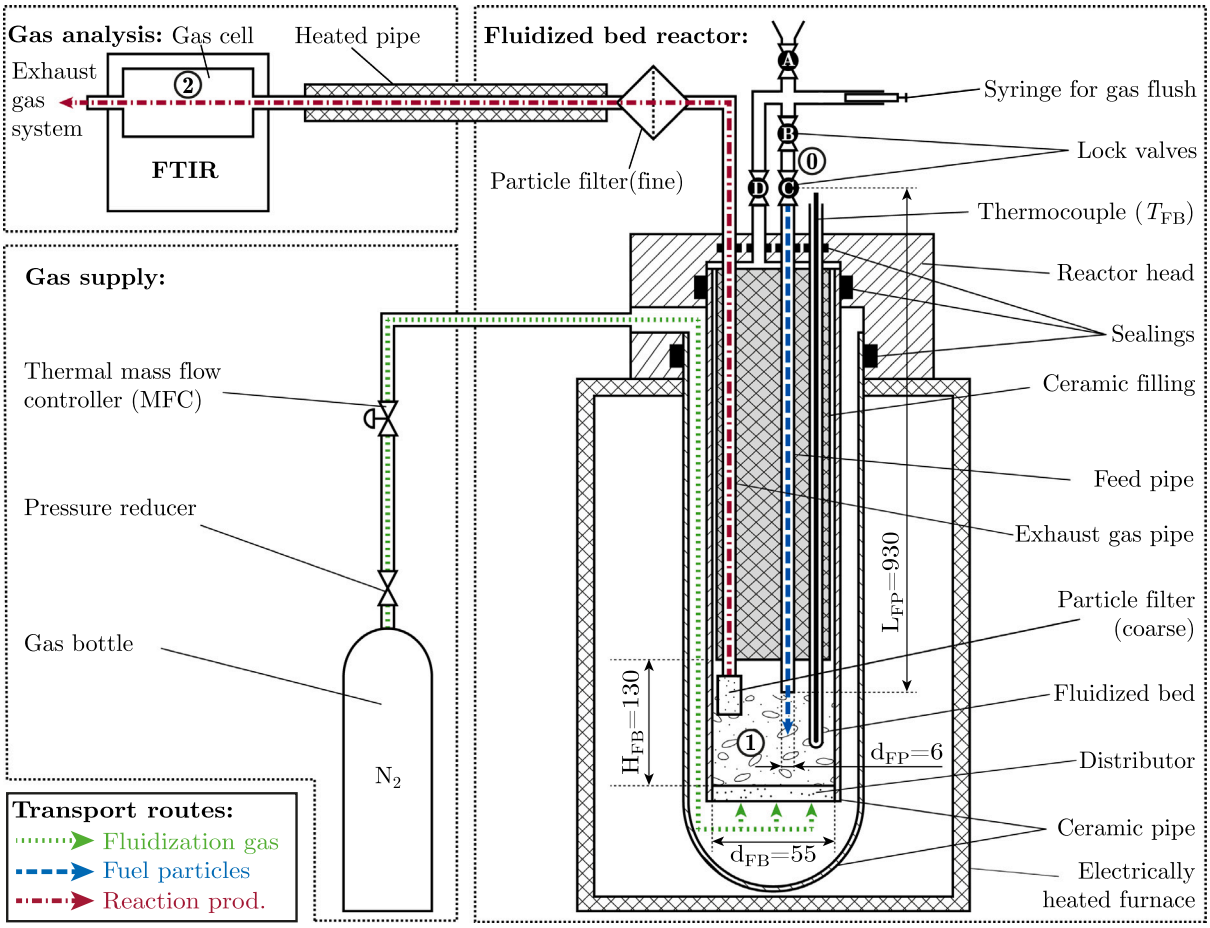

Fig. 1. Scheme of the fluidized bed reactor setup for pyrolysis experiments [39]. (For interpretation of the references to color in this figure legend, the reader is referred to the web version of this article.)

Table 1
Physical and chemical properties of the investigated isolated biomass components cellulose (Cel.), hemicellulose (Hem.), and lignin (Lig.) using ultimate, proximate, and microscopic particle size analysis [39].

			Cel.	Hem.	Lig.
C	[wt%]	daf[b]	42.43	41.12	60.69
H	[wt%]	daf	6.32	6.23	5.57
N	[wt%]	daf	0.30	0.21	1.22
S	[wt%]	daf	0.00	0.10	0.81
O[a]	[wt%]	daf	50.95	52.34	31.71
Ash	[wt%]	dry	0.30	2.00	1.30
Water	[wt%]	aa[c]	6.00	3.50	4.10
Volatiles	[wt%]	daf	95.19	76.13	68.19
$d_{p,10}$	[µm]		135.8	71.3	114.7
$d_{p,50}$	[µm]		164.8	93.7	125.9
$d_{p,90}$	[µm]		195.4	114.7	158.0

[a] From difference.
[b] Reference state: dry, ash-free.
[c] Reference state: as analyzed.

allow the reaction atmosphere and temperature to be adjusted independently. The fluidized bed ensures good heat and mass transfer and homogeneous boundary conditions over time and space. In the above-mentioned study, pyrolysis experiments were carried out in a pure N_2 atmosphere in a temperature range of 573–973 K. Pulverized samples of the extracted biomass structural components with masses between 15 and 50 mg were injected batch-wise from position ⓪ via a double-lock system into the reaction zone in the fluidized bed, marked as position ① and shown with a blue line in Fig. 1. The fuel transport was supported by a gas flush (also N_2) from a syringe to prevent particles from sticking to the feed tube walls, to ensure high particle heating rates in the range of 10^4–10^5 K s^{-1}, and to minimize the reaction time within the feed tube under conditions other than those provided by the fluidized bed. After reaching the bed, the particles remain there until final conversion. All the gaseous reaction products (volatiles) that are released mix with the fluidization gas and leave the reactor through an exhaust pipe before passing the FTIR gas cell (red line). There, the volume fractions $\varphi_i(t)$ of 22 different IR-active gas species are measured simultaneously with a time resolution of 10 Hz [39]. From these volume fractions, the time-dependent total volatile release rate

$$\frac{\mathrm{d}y_{\mathrm{vol,exp}}(t)}{\mathrm{d}t} = \sum_{i=1}^{22}\left(\frac{\rho_{\mathrm{N_2,n}}\cdot M_{\mathrm{i}}}{M_{\mathrm{N_2}}}\cdot\frac{\dot{V}_{\mathrm{N_2,n}}}{m_0}\cdot\frac{\varphi_{\mathrm{i}}(t)}{1-\sum_{j=1}^{22}\varphi_{\mathrm{j}}(t)}\right) \quad (1)$$

is derived. The first term contains constants (N_2 density at standard conditions $\rho_{N_2,n}$, molar mass M,) that are identical for all experiments. The variables given in the second term (volume flow $\dot{V}_{N_2,n}$, sample mass m_0) are parameters of the respective test series. They are adjusted to the temperature and fuel reactivity but remain constant within an individual experiment. The third term contains the time-dependent volume fractions $\varphi(t)$, measured individually for every single experiment. It should be noted that the rates are observed in the gas cell. They cannot be compared directly with the release rate at the particle, instead, suitable models (see Section 3.4) must be used to reflect the transport behavior between the reaction zone and the analyzer.

The working principle of the experimental setup for the determination of the kinetic data has been proven in advance both experimentally [45] and theoretically [46], with special emphasis on the

limitations resulting from the gas transport between the reaction zone and the analyzer. All experimental reference data are available online (10.18154/RWTH-2021-05544 [47]).

3. Modeling

In this study, three models of varying complexity are evaluated in terms of the predictability of the volatile release during the pyrolysis of extracted and separated biomass components. In order of increasing complexity, they are the single first-order model (SFOR), the chemical reaction engineering and chemical kinetics model (CRECK), and the chemical percolation devolatilization model (CPD).

3.1. Single first-order model (SFOR)

The SFOR model is the least complex model. In this model, the solid conversion rate

$$\frac{\mathrm{d}y_\mathrm{s}}{\mathrm{d}t} = -r(T) \cdot \left[y_\mathrm{s}(t) - y_{\mathrm{s},\infty}(T)\right]. \tag{2}$$

is proportional to the remaining fraction of reactive material – given by the difference between the actual solid yield $y_\mathrm{s}(t)$ and the final solid yield fraction $y_{\mathrm{s},\infty}(T)$ as a function of the temperature – and the global characteristic reaction rate r. Typically, the temperature dependency of the reaction rate is taken into consideration using an Arrhenius approach

$$r(T) = A \cdot \exp\left(\frac{-E_\mathrm{a}}{R \cdot T}\right) \tag{3}$$

involving the pre-exponential factor A, the activation energy E_a, and universal gas constant R. Due to its simplicity, the SFOR model cannot account for the complex chemistry of biomass pyrolysis with different bond types, multiple competing reactions, or intermediate species. Nevertheless, its reasonable description of the process, combined with its low numerical cost, makes it a popular model for use in CFD simulations of large-scale systems, such as combustion chambers [48–51] or pyrolysis apparatuses [52], where the focus is on understanding the overall process or designing and optimizing entire systems. In stand-alone investigations of laboratory-scale pyrolysis experiments, the model is mostly used as reference for more complex single-particle pyrolysis models. As the SFOR model is fuel-dependent, it always needs to be calibrated with either experimental reference data or predictions from more sophisticated pyrolysis models. In this study, the SFOR model is calibrated against the experimentally obtained total volatile release rates (see Eq. (1)) from the fluidized bed reactor.

3.2. Chemical reaction engineering and chemical kinetics model (CRECK)

The CRECK model (in this study the version CRECK-S-2003-Bio) is a multi-step, branched kinetic mechanism first described by Ranzi et al. [23] and updated by Debiagi et al. [24]. Biomass is assumed to consist of various reference components: not only cellulose but also different types of hemicellulose and lignin and some representatives of extractives. The model includes chemisorbed intermediate lumped species but produces clearly defined molecular species (permanent light gases and condensable components) and residual char. Fig. 2 gives an overview of the product species and reaction pathways of the three main components cellulose, hemicellulose (xylan), and lignin.

Each reaction is assumed to progress individually with a single first-order reaction characterized by the reaction rate r_i. The corresponding reaction rate is modeled with an Arrhenius approach (Eq. (3)). All parameters (pre-exponential factor A_i, activation energy $E_\mathrm{a,i}$ and stoichiometric factors) are listed in Debiagi et al. [24]. As the hemicellulose used in the experiments is xylan extracted from beech wood [39], the model scheme only shows the reaction pathways of hardwood xylan. In total, the reaction mechanism for cellulose includes 22 species and 8 reactions, the one for hemicellulose has 32 species and 13 reactions, and the one for lignin features 33 species and 16 reactions. For comparison with the Bio-CPD model, all species are categorized either as tar or light gas. Tar includes all hydrocarbons with either more than four carbon atoms or the presence of an oxygen atom (not including CO, CO_2 and H_2O).

3.3. Chemical percolation devolatilization model (CPD)

The chemical percolation devolatilization model (CPD) originally developed for coal [6–8] – like the version adapted for biomass (Bio-CPD) [31–34,53] – is a phenomenologically based pyrolysis model that attempts to include the chemical-physical processes in the particle and the molecular structure, respectively. The model assumes the solid to be a network of aromatic macromolecules linked together by means of various chemical bonds. The bonds between the aromatic ring structures have different levels of stability and are grouped into labile and stable bridges. Labile bridges can be converted into stable bridges during the pyrolysis process or break apart to form side chains.

Fig. 3 illustrates the reaction steps and names the corresponding reaction rates in the population modeling for the bridge fractions X_i according to the following differential equations for labile bridges

$$\frac{\mathrm{d}X_\mathrm{lab}}{\mathrm{d}t} = -r_\mathrm{lab} \cdot X_\mathrm{lab}, \tag{4}$$

activated bridges

$$\frac{\mathrm{d}X_\mathrm{act}}{\mathrm{d}t} = r_\mathrm{lab} \cdot X_\mathrm{lab} - (r_\mathrm{stab} + r_\mathrm{SC}) \cdot X_\mathrm{act}, \tag{5}$$

stable bridges

$$\frac{\mathrm{d}X_\mathrm{stab}}{\mathrm{d}t} = r_\mathrm{stab} \cdot X_\mathrm{act} \tag{6}$$

and side chains

$$\frac{\mathrm{d}X_\mathrm{SC}}{\mathrm{d}t} = 2 \cdot r_\mathrm{SC} \cdot X_\mathrm{act} - r_\mathrm{LG} \cdot X_\mathrm{SC}. \tag{7}$$

All reaction rates r_i (the ratio of r_SC to r_stab is named r^*) are modeled using an Arrhenius approach with activation energies distributed according to a Gaussian profile characterized by the mean $\mu_{E_\mathrm{a,i}}$ and the standard deviation $\sigma_{E_\mathrm{a,i}}$ as a function of the reaction progress. Table 2 lists these parameters for all three biomass components in conjunction with the initial population of intact ($X_{\mathrm{int},0}$) and stable ($X_{\mathrm{stab},0}$) bridges. A previous study found that out of the four proposed sets of parameters that are available in the literature [31,32,34,53] for each component, the listed ones best describe the reaction behavior under the boundary conditions of the fluidized bed reactor [55]. For lignin, the kinetic parameter set originally derived for coal, as proposed by Grant et al. [6] and the Genetti correlation [56], designed to estimate structural parameters based on proximate and ultimate analysis data, are used in combination as this showed the best performance in comparison with the parameter sets found in the literature [55].

According to the percolation theory (PT), the bridge population is used as an input to compute the mass fractions of finite fragments that are separated from the infinite char matrix. The probability P_{N_cl} of finding fragments with a particular number of aromatic clusters N_cl is determined by the fractions of intact X_int and broken bridges X_bro as well as the number of possible configurations N_conf:

$$P_{N_\mathrm{cl}} = N_\mathrm{conf} \cdot X_\mathrm{int}^{N_\mathrm{int}} \cdot X_\mathrm{bro}^{N_\mathrm{bro}}. \tag{8}$$

The number of possible configurations is calculated under the assumption of a Bethe lattice (no ring structures) using the correlation developed by Fisher and Essam [57]:

$$N_\mathrm{conf} = \frac{\sigma + 1}{N_\mathrm{int} + N_\mathrm{bro}} \cdot \underbrace{\left(\frac{\Gamma(N_\mathrm{cl} \cdot \sigma + 2)}{\Gamma(N_\mathrm{cl}) \cdot \Gamma(N_\mathrm{bro} + 1)}\right)}_{\binom{N_\mathrm{int} + N_\mathrm{bro}}{N_\mathrm{int}}}, \tag{9}$$

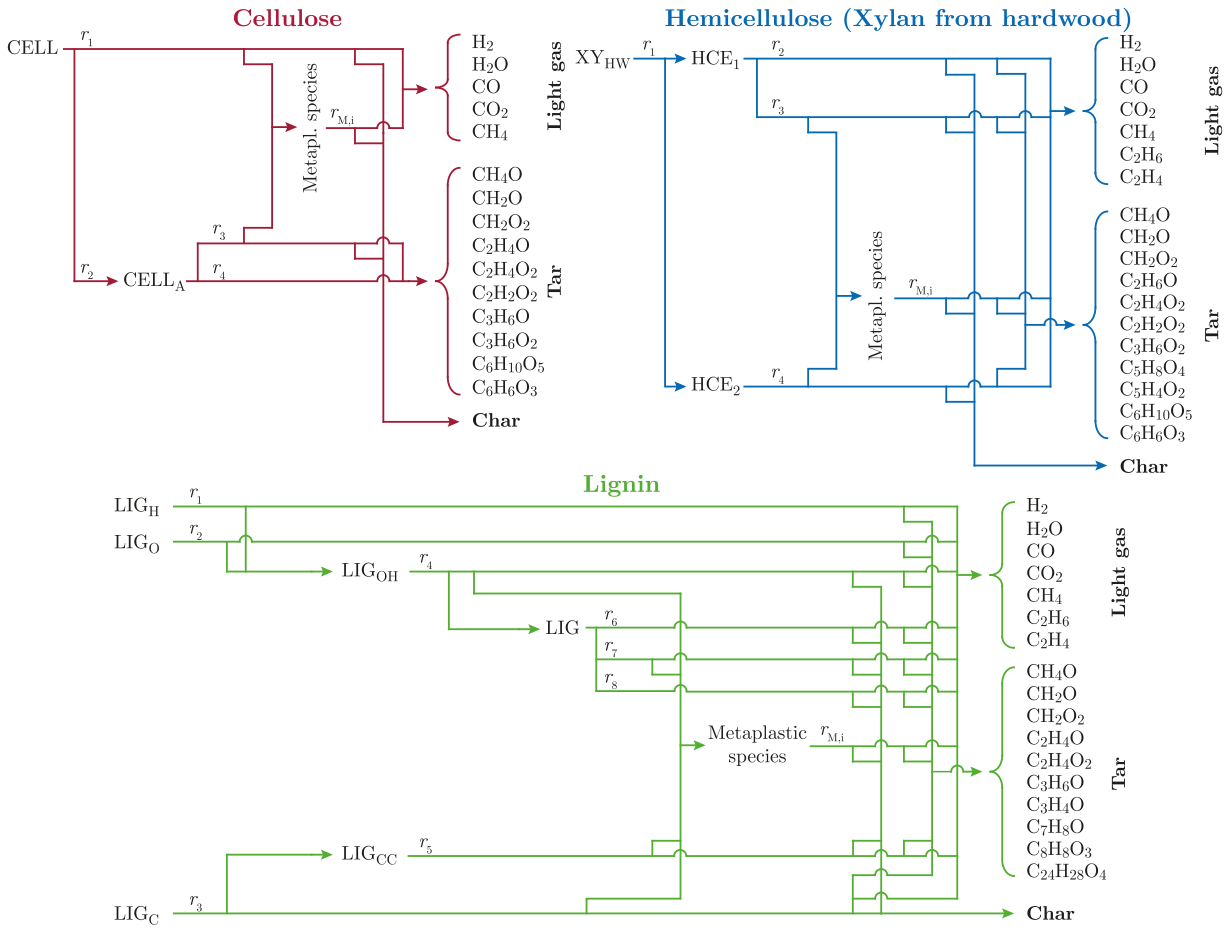

Fig. 2. Reaction pathways of the CRECK model.
Source: Based on Debiagi et al. [24].

Table 2
Structure and kinetic parameters of the Bio-CPD model evaluated as best fitting parameter combinations for the fluidized bed reactor [55].

		Cel.[a]	Hem.[b]	Lig.[c]
m_{cl}	[u]	162	162	380.7
m_{SC}	[u]	15.96	37	57.98
$X_{int,0}$	[−]	0.999	0.999	0.65
$X_{stab,0}$	[−]	0	0	0.15
σ	[−]	1.005	1	1.85
A_{lab}	$[s^{-1}]$	$2.14 \cdot 10^{15}$	$1 \cdot 10^{18}$	$2.6 \cdot 10^{15}$
$\mu_{E_{a,lab}}$	$[kJ\,mol^{-1}]$	226.38	215.62	231.79
$\sigma_{E_{a,lab}}$	$[kJ\,mol^{-1}]$	11.145	10.467	7.531
A_{LG}	$[s^{-1}]$	$1.19 \cdot 10^{8}$	$5 \cdot 10^{12}$	$3.0 \cdot 10^{15}$
$\mu_{E_{a,LG}}$	$[kJ\,mol^{-1}]$	111.97	159.93	288.70
$\sigma_{E_{a,LG}}$	$[kJ\,mol^{-1}]$	3.680	20.934	33.890
A_{r^*}	[−]	3.02	0.01	0.9
$\mu_{E_{a,r^*}}$	$[kJ\,mol^{-1}]$	0	−20.52	0

[a] Data set derived by Vizzini et al. [32].
[b] Data set derived by Sheng and Azevedo [31].
[c] Kinetic parameters proposed by Grant et al. [6] for fossil fuels in combination with the Genetti correlation [56].

where $N_{int} = N_{cl} - 1$ and $N_{bro} = N_{cl} \cdot (\sigma - 1) + 2$ represent the numbers of intact and broken bridges in the corresponding fragment as a function of the coordination number σ. The Eulerian gamma function Γ is required to represent the binomial coefficient even for a non-integer N, resulting from averaging different lattices.

To calculate the mass fractions $y_{frag,N_{cl}}$, it is necessary to consider the molecular structure of the fragments, which is described by the molecular weights (m_i) of the building blocks. Eq. (10) gives the change in mass fraction for a given fragment size class (consisting of N_{cl} clusters) caused by variations in the bridge population based on the principles of percolation theory [54]:

$$\frac{dy_{frag,N_{cl},PT}}{dt} = \frac{d}{dt}\left[\frac{P_{N_{cl}}}{N_{cl}\cdot m_{cl}}\cdot\left(\underbrace{N_{cl}\cdot m_{ar}}_{\substack{\text{mass of}\\ \text{aromatic rings}}} + \underbrace{N_{int}\cdot m_{lab}\cdot\frac{X_{lab}}{X_{int}}}_{\substack{\text{mass of}\\ \text{intact bridges}}} + \underbrace{N_{bro}\cdot m_{SC}\cdot\frac{\frac{X_{SC}}{2}}{X_{bro}}}_{\substack{\text{mass of}\\ \text{side chains}}}\right)\right]. \tag{10}$$

As depicted in Fig. 3, the finite fragments that are forecasted using the percolation theory can undergo further reaction steps: reattachment to the infinite char matrix (cross-linking) or evaporation and outgassing from the particle. Eq. (11) controls the overall change rate of the fragments:

$$\underbrace{\frac{dy_{frag,N_{cl}}}{dt}}_{\text{overall change}} = \underbrace{\frac{dy_{frag,N_{cl},PT}}{dt}}_{\text{source from PT}} - \underbrace{\frac{dy_{frag,N_{cl},cross}}{dt}}_{\text{cross-linking}} - \underbrace{\frac{dy_{frag,N_{cl},ext}}{dt}}_{\text{particle release}}. \tag{11}$$

The aggregate state of the fragments (liquid or gaseous) decides which reaction path is possible for the respective fragment. While fragments in the liquid phase are able to crosslink with the infinite char matrix,

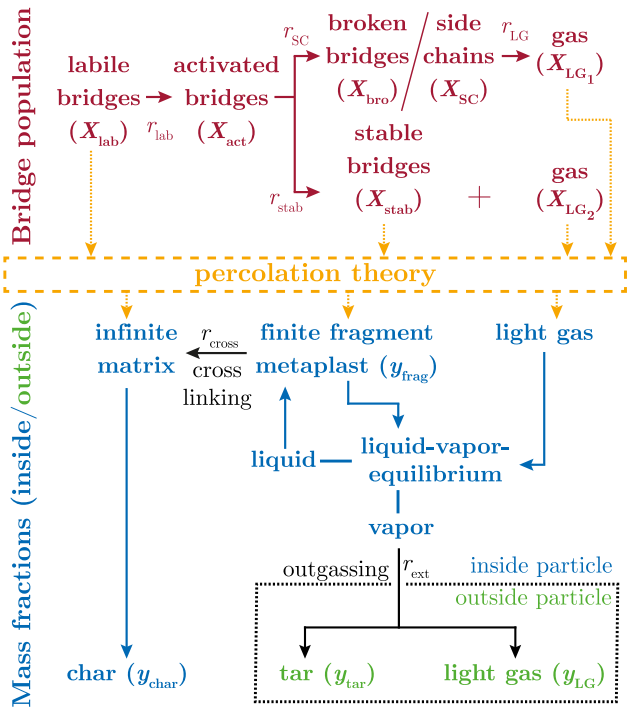

Fig. 3. Structure, reaction pathways and variable names of the Bio-CPD model [54,55].

only gaseous fragments can be released from the particle. Thus, a vapor–liquid equilibrium (VLE), as developed by Fletcher et al. [8] and based on the principles proposed by King [58], is used to split the mass fractions of fragments $y_{frag,N_{cl}}$ into a liquid fraction $y'_{frag,N_{cl}}$ and a gaseous fraction $y''_{frag,N_{cl}}$. The calculation of the VLE takes into consideration the effects of the temperature, pressure, and fragment size.

The rate of cross-linking is then formulated for the liquid fraction using Eq. (12) :

$$\frac{dy_{frag,N_{cl},cross}}{dt} = r_{cross} \cdot y'_{frag,N_{Cl}}. \tag{12}$$

The cross-linking reaction rate r_{cross} is modeled with an Arrhenius approach ($A_{cross} = 3 \cdot 10^{15}\,s^{-1}$, $E_{a,cross} = 272.14\,kJ\,mol^{-1}$ [8]). For simplicity, the reaction rate is assumed to be the same for all fragments, although larger fragments have a higher crosslinking probability due to either their larger number of side chains or the fragments from different biomass components may exhibit different functionalities.

In contrast to the liquid fractions, the gaseous fractions can leave the particle. This is also modeled via a differential equation:

$$\frac{dy_{frag,N_{cl},ext}}{dt} = r_{ext} \cdot y''_{frag,N_{cl}}. \tag{13}$$

Here, the rate of external release r_{ext} controls how gaseous fragments inside the particle are transported to the surrounding gas phase. In principle, the quantity and rate of fragments released from the particle depend on the internal particle structure (porosity) and the particle size. The larger the particle, the larger the internal transport resistance and the lower the tar yield [59]. This study only investigates pulverized particles (see Table 1) with particle diameters $d_p < 200\,\mu m$. Taking the rate $r_{ext} \leq 10^5\,s^{-1}$, internal transport processes are considered to be much faster than all chemical reaction steps. Once released from the particle, the fragments of all different size classes are cumulated and treated as tar.

In addition to the released fragments, the CPD model also predicts a light gas fraction originating from the bridge stabilization reaction and from side chains splitting off. The fraction of bridges already transferred to light gas can be expressed using Eq. (14):

$$X_{LG} = \underbrace{2 \cdot X_{bro} - X_{SC}}_{X_{LG_1}} + \underbrace{2 \cdot \left(X_{stab} - X_{stab,0}\right)}_{X_{LG_2}}. \tag{14}$$

If the molecular weights of the cumulated released light gas are placed in relation to the initial total molecular weight of the network, the change rate of the mass-based light gas fraction $y_{LG,PT}$ can be expressed:

$$\frac{dy_{LG,PT}}{dt} = \frac{d}{dt}\left[\frac{\overbrace{m_{SC} \cdot \frac{X_{LG}}{2} \cdot (\sigma + 1) \cdot \left(1 - y_{tar}\right)}^{\text{cumulated light gas molecular weight}}}{\underbrace{m_{ar} + m_{SC} \cdot (\sigma + 1) \cdot \left(1 - X_{stab,0}\right)}_{\text{initial total molecular weight}}} \right]. \tag{15}$$

The term $\left(1 - y_{tar}\right)$ represents the release of potential light gas sources due to the release of fragments designated as tar. The released fragments still have the potential to be further decomposed in the gaseous phase or to split off side chains. However, since the released fragments may be subject to temperature boundary conditions that are different than the particle temperature, the light gas release due to these decomposition processes is not taken into account in the CPD model. However, this effect is handled by the tar cracking model. Further on, light gas is assumed to always be in the gaseous phase and to be released with the same release rate r_{ext} as the fragments.

Keeping all model formulations in a purely differential notation means they can easily be coupled with the particle model and the reactor model, respectively [54].

3.4. Particle model and reactor model

All the pyrolysis models described above require a temperature as an input parameter. For the primary pyrolysis models, the particle temperature T_p is required. This is derived from a particle model coupled bidirectionally with the pyrolysis model. As the comparison with the experimental data determined from *ex-situ* measurements is not possible at the particle level, the particle model and pyrolysis model are further coupled bidirectionally with a gas-phase model that takes into account transport phenomena and secondary gas-phase reactions.

Particle mass and energy balance

The particle temperature is calculated from an energy balance around one single fuel particle approximating the boundary conditions of the experimental setup. In Eq. (16), the differential equation for the transient homogeneous particle temperature is given considering convective heat transfer, radiation, and reaction enthalpies:

$$\begin{aligned} \underbrace{m_p \cdot c_p \cdot \frac{dT_p}{dt}}_{\text{heat-up}} &= \underbrace{\alpha \cdot S_p \cdot \left(T_g - T_p\right)}_{\text{convection}} + \underbrace{\frac{dm_p}{dt} \cdot \Delta h_{reac}}_{\text{reaction}} \\ &+ \underbrace{\sigma \cdot S_p \cdot \left(\frac{1}{\varepsilon_p} + \frac{1}{\varepsilon_{FB}} - 1\right)^{-1} \cdot \left(T_{FB}^4 - T_p^4\right)}_{\text{radiation}} \end{aligned} \tag{16}$$

Here, m_p is the particle mass of one single representative fuel particle derived from the mass balance (Eq. (17)) and c_p is the particle's specific heat capacity estimated using the correlation proposed by Merrick [60]. The convective heat transfer coefficient α is calculated based on the Nusselt correlation provided by Gunn [61] for single spherical particles intermixed in a fluidized bed. The particle surface area S_p is calculated for a representative spherical particle with a constant diameter $d_p = d_{p,50}$ according to the microscopic particle size analysis given in Table 1. The gas temperature T_g and the bed temperature T_{FB} are equal to the oven set temperature and are cross-checked with the

thermocouple in the reaction zone (see Fig. 1). The radiative heat transfer is modeled according to Lienhard I.V. and Lienhard V. [62] with an apparent bed emissivity $\varepsilon_{FB} = 0.7$, a particle emissivity $\varepsilon_p = 0.8$ and the Stefan–Boltzmann constant σ. The reaction term with the specific reaction enthalpy $\Delta h_{reac} = 418.4\,kJ\,kg^{-1}$ takes into account the heat sink due to the endothermic pyrolysis reaction. Apart from endothermic reactions, also exothermic pyrolysis reactions (especially lignin) have been reported [63]. However, the effect of reaction enthalpy on the observed volatile release rates is small [55].

As the particle mass influences the heat-up process, the transient particle mass m_p is calculated with the mass balance

$$\frac{dm_p}{dt} = \underbrace{m_{p,0} \cdot \left(1 - y_{a,0}\right)}_{\text{initial reaction mass } m_{reac,0}} \cdot \frac{dy_{vol}}{dt}. \tag{17}$$

The mass change rate is derived from the initially available reactive mass by excluding the ash mass and the volatile release rate $\frac{dy_{vol}}{dt}$ extracted from one of the pyrolysis models introduced in Sections 3.1 to 3.3.

Gas transport

The particle model is coupled with a gas-phase model to take into account the gas transport from the reaction zone in the fluidized bed to the gas analysis in the FTIR gas cell, as well as secondary reactions of the primary pyrolysis products. Thus, the released volatiles are embedded as a source term in a 1D gas-phase model as described by the following differential equation:

$$\frac{dm_{i,j}}{dt} = \underbrace{\dot{m}_i(t) \cdot \left(\frac{m_{i-1,j}}{m_{i-1,tot}} - \frac{m_{i,j}}{m_{i,tot}}\right)}_{\text{advective mass transfer}} + \underbrace{N_p \cdot m_{reac,0} \cdot \frac{dy_j}{dt} \cdot B_i}_{\text{source from particles}} \pm \underbrace{\frac{dm_{i,j,GPR}}{dt}}_{\text{gas-phase reaction}} \tag{18}$$

The advective term results from the mass transport due to the fluidizing N_2 gas flow and the gas flush during the particle injection phase. Products and fluidization gas are assumed to be perfectly mixed within each cell of the 1D model. Further on, isobar conditions are assumed. The source term from the pyrolysis model is multiplied by the number of particles N_p and a Boolean function that controls the release of volatile only in the fluidized bed cell.

Gas phase reactions

Depending on the pyrolysis model, different approaches are used to model the effect of secondary gas-phase reactions. While the Bio-CPD model only provides the lumped products light gas and tar as output variables, the CRECK model predicts single species with known molecular formulas. Thus, for simulations using the Bio-CPD model a single first-order tar cracking approach is used that converts tar into light gas depending on the local gas temperature $T_{g,i}$ given by the 1D model:

$$\frac{dm_{i,tar,GPR}}{dt} = -A_{tar,GPR} \cdot e^{-\frac{E_{a,tar,GPR}}{R \cdot T_{g,i}}} \cdot m_{i,tar} = -\frac{dm_{i,LG,GPR}}{dt} \tag{19}$$

The parameter sets developed by Fagbemi et al. [64] ($A_{tar,GPR} = 4.34\,s^{-1}$ $E_{a,tar,GPR} = 23.4\,kJ\,mol^{-1}$) and by Pielsticker and Kneer [55] (Cellulose/Hemicellulose: $A_{tar,GPR} = 1.58 \cdot 10^3\,s^{-1}$, $E_{a,tar,GPR} = 38.06\,kJ\,mol^{-1}$, Lignin: $A_{tar,GPR} = 6.71\,s^{-1}$, $E_{a,tar,GPR} = 18.20\,kJ\,mol^{-1}$) are used to analyze the effect of secondary tar cracking reactions.

For simulations using the CRECK model, a detailed gas-phase reaction mechanism is used, with 339 species and 9781 reactions (CRECK-G-2003 [22,65,66]) considered. Due to the higher complexity, a direct coupling to the 1D model from Eq. (18) is not possible. Instead of considering the effects of secondary gas-phase reactions and gas transport simultaneously, two separate modeling approaches are used to cover these aspects. First, the detailed gas-phase reaction mechanism is calculated for fixed conditions, and second, the gas transport is calculated with a convolution function, which is based on the Aris-Taylor dispersion theory as proposed by Abad et al. [67]. For simplification, all reactions take place under a constant reaction temperature equal to the bed temperature T_{FB} of the corresponding experiment for a previously fixed gas residence time. The gas residence time is taken from the 1D simulation, taking into consideration different temperatures and volume flows in the FBR and ranges between 1.03 and 2.97 s. The convolution function also considers the effects of temperature and volume flow on the transport behavior, but neglects any reactions on the way from the reaction zone to the FTIR gas cell.

4. Results

To achieve a comprehensive comparison of the predictivity and performance of the different models, aspects regarding the heating rate are addressed by comparing TGA data (Section 4.1) and FBR data (Sections 4.2 to 4.4) while Sections 4.2 and 4.3 focus on the different model outputs: the volatile release rate and the final yield. Section 4.4 highlights the relevance of secondary gas-phase reactions. All simulation results are provided as open-access data [68].

4.1. Conversion during thermogravimetric analysis

Fig. 4 shows the fraction of remaining solid during the thermogravimetric analysis for the three individually investigated biomass components. The experimental reference values come from Pielsticker et al. [39] and were recorded with a constant heating rate of $5\,K\,min^{-1}$. The different-colored lines represent the model predictions using the SFOR, CRECK, and Bio-CPD models.

Overall, the models can predict the decomposition of cellulose better than that of the compared other fuels. The main reason is the comparatively simple molecular structure of cellulose, which is characterized by high linearity and a limited number of different bond types. Nevertheless, non-negligible deviations can be found between the model predictions and the experimental reference data. One aspect is that all models predict a slightly later onset of the reaction (shift in the moment that the yield drops as the temperature rises) and a slightly lower reactivity (lower gradient) compared to the experimental data. The CRECK model makes the most accurate prediction while that of the Bio-CPD model is least accurate. The main reason might be that the kinetics of the CRECK model are calibrated against experimental data from TG experiments [23,69], while the Bio-CPD parameters used for cellulose are derived from experiments at high heating rates in a fluidized bed reactor [32]. The tendency for the reaction to start slightly later is already seen in the study by Ranzi et al. [23].

The models' predictions also differ in terms of the final remaining char yield. The Bio-CPD model already reaches full conversion at approximately 700 K and thus does not leave any solid residue. In contrast, the amounts of final residues left by the SFOR model ($y_{s,\infty} = 6.8\%$) and the CRECK model ($y_{s,\infty} = 8.7\%$) are slightly above the final char yield obtained experimentally ($y_{s,\infty} = 3.6\%$). The complete decomposition of cellulose in the Bio-CPD model results from the network structure that is assumed to result from the high linearity ($\sigma = 1.005$), low number of initially available stable char bridges ($X_{stab,0} = 0$) and high proportion of bridge-breaking reactions ($A_{r^*} = 3.02$) compared to stabilization reactions. Cross-linking reactions cannot compensate for this effect. The same effect is also found in the final yields of the fluidized bed experiments in Fig. 6, as discussed later.

Similar assumptions about the network structure of hemicellulose ($\sigma = 1$, $X_{stab,0} = 0$) compared to cellulose lead to a similarly strong overestimation of pyrolytic decomposition by the Bio-CPD model. This is compensated for to some extent by the temperature-dependent reaction rate ratio r^*, which favors a stabilization reaction at higher temperatures and results in a marginal final yield of 2.0%. Similar

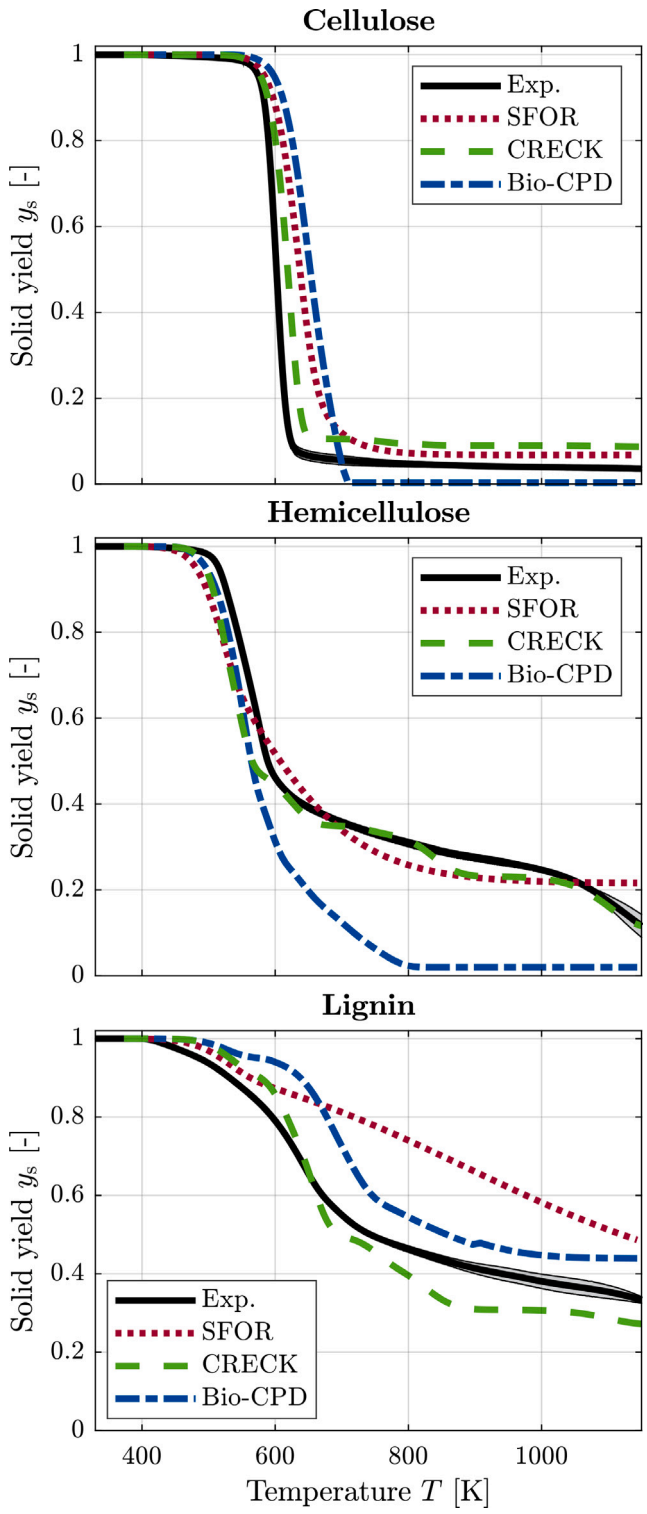

Fig. 4. Experimentally obtained solid mass fraction as a function of temperature (fixed heating rate 5 K min^{-1}) [39] in comparison with predictions from SFOR, CRECK, and Bio-CPD models for the three extracted components cellulose, hemicellulose, and lignin. The gray-shaded area marks the deviation obtained between repeated runs.

observations of the Bio-CPD model overestimating the volatile yield have also been made by Xing et al. [38]. Although the final yield predicted by the SFOR model ($y_{s,\infty}$ = 21.6%) is comparatively higher than the experimental one ($y_{s,\infty} \approx$ 11%), it can reproduce the reaction progress within the scope of its possibilities very well over a wide temperature range. The offset mainly results from a second reaction step above 1000 K, which cannot be captured by the simplified model structure of the SFOR model with only one global reaction rate. The CRECK model is the only model that can capture the entire reaction progress including the second reaction step above 1000 K. Detailed analysis of the CRECK model reveals that this release mainly results from the metaplastically trapped species COH_2 (see Fig. 2), which is released from the particle as CO, H_2 and H_2O at temperatures above 1000 K.

All models predict a slightly earlier onset of the reaction for hemicellulose compared to cellulose and lignin. One potential reason for this might be that some model parameters are calibrated based on biomasses where all three components are coexistent. Thus, some effects might be compensated for by another component. There may also be small differences between the actual sample temperature and the measured temperature.

The CRECK and Bio-CPD models' predictions for lignin are in a similar range of accuracy compared to the experimental data. By contrast, the SFOR model shows a significantly lower decomposition, especially at higher temperatures. The molecular structure of lignin with a lot of different bond types is too complex to be modeled with only one characteristic reaction rate. The procedure to calibrate the SFOR model for lignin to the experimentally obtained total volatile release rates from the fluidized bed reactor is mainly driven by the fast reactions, as they are responsible for the peak in the release rate. Slow reactions only have a minor impact on the derivative and are thus taken into account to a lower extent in the calibration process [39].

In summary for the TGA experiments, the CRECK model predictions are closest to the experimental results. The reason for this is that it is calibrated against TGA experimental data gained with extracted and separated basic biomass components. The SFOR model shows satisfying results for the decomposition of solids with comparatively simple molecular structures such as cellulose or hemicellulose, where the amount of different chemical reactions is limited and the decomposition is characterized by a distinct peak in the DTG curve. Once the molecular structure gets more complex and the diversity of bond types increases, the prediction by the SFOR model deviates considerably. The Bio-CPD model is mainly not well suited describing the decomposition in the case of pyrolysis with slow heating rates. As this model was originally developed for flash pyrolysis with high heating rates and temperatures, the reaction pathways for a slow heat-up (especially stabilization reactions and cross-linking) might not be well calibrated. Of all the fuels, the Bio-CPD model shows the lowest deviation from the experiments for lignin. As the molecular structure of lignin is closest to that of fossil fuels, this indicates that improvements may have to be undertaken for molecules with a low degree of connectivity.

4.2. Total volatile release rates in the fluidized bed reactor

Fig. 5 shows the total volatile release rate $\frac{dy_{vol}}{dt}$ obtained experimentally from concentration measurements in the FTIR gas cell and subsequent evaluation with Eq. (1) in comparison to predictions from the SFOR, CRECK, and Bio-CPD models. Since the experimental data are only available for the analyzed location, gas transport effects from the reaction zone to the gas cell have been taken into account for all model predictions. As only the total volatile release rate is compared here, it is not necessary either to differentiate between into individual product classes or to take into account secondary gas-phase reactions in the models. While the CRECK and Bio-CPD models do not use any of the experimental data from the FBR for calibration and are thus entirely predictive, the SFOR model uses the total volatile release rate as calibration data and can thus only be regarded as descriptive.

The most obvious finding is that the CRECK model tends to overestimate the total volatile release rate. In particular, the release rates for lignin are overestimated at all three operating temperatures. Those for cellulose show good agreement at 973 K but are overpredicted at

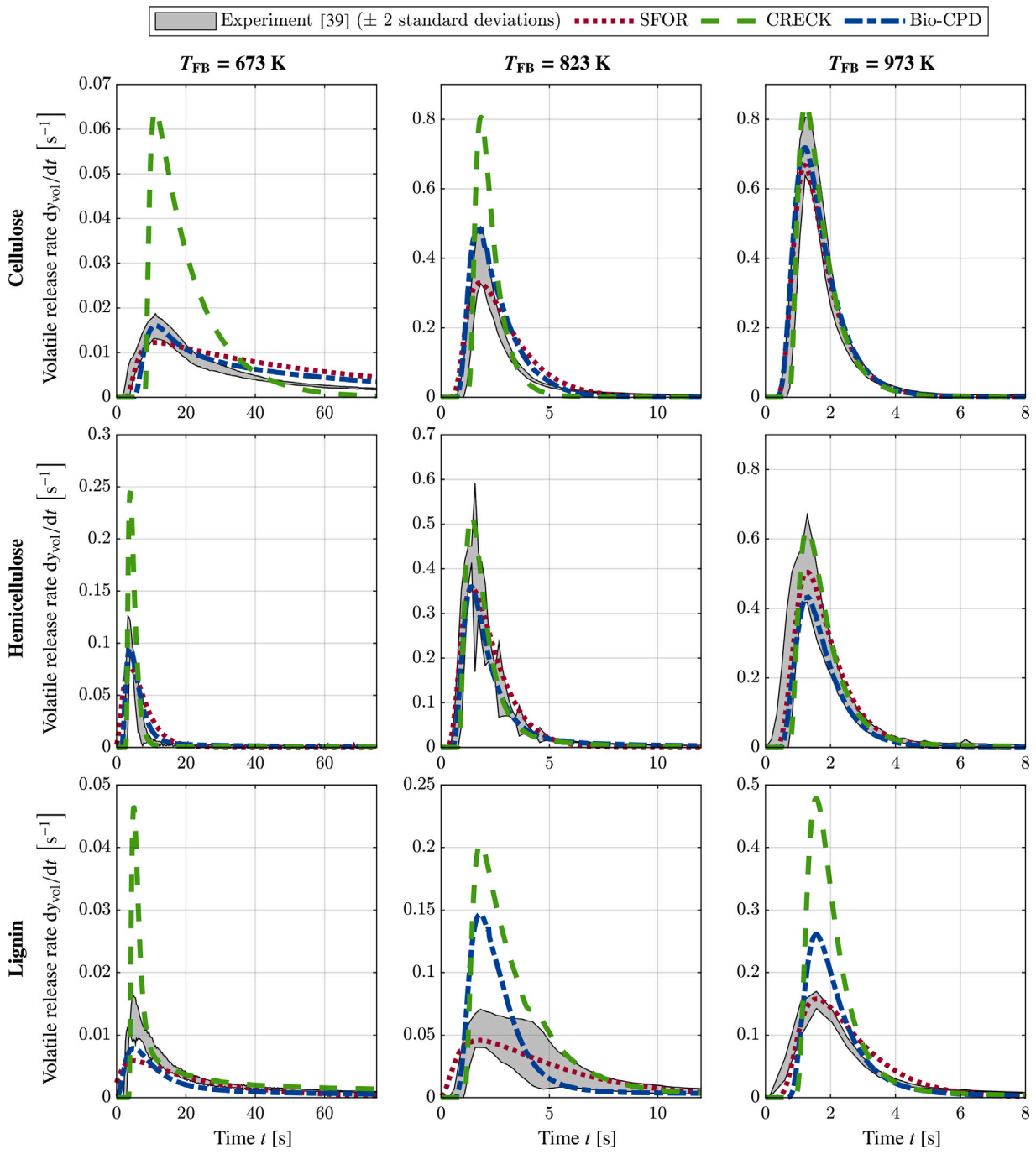

Fig. 5. Experimentally obtained volatile release rates in the FTIR gas cell at different fluidized bed reactor temperatures [39] in comparison with predictions from SFOR, CRECK, and Bio-CPD model for the three biomass components cellulose, hemicellulose, and lignin. The gray-shaded area marks the double standard deviation obtained during multiple repetitions of single batch experiments.

lower temperatures. The release rates for hemicellulose are only over-predicted in the 673 K case. This is unlikely to be due to intraparticle transport processes not considered in the model (assumption of Biot number Bi $\ll$ 1) or to the limitations of heat transfer compared to the particles' required heat of reaction (pyrolysis number Py $\gg$ 1), since the simulated reaction time is significantly larger than the heating time. As the final yields (see Fig. 6) are captured quite well with the CRECK model, these results indicate that the kinetic parameters of key reactions should be recalibrated to improve the rate predictions. It should be noted that a common approach with two competing reactions to cover different reaction rates in the high- or low-temperature regimes will not achieve the desired effect of decreasing reactivity. Decreasing the pre-exponential factor of key lignin reactions and adjusting the activation energies of key hemicellulose and cellulose reactions would make it possible to capture the measured release rates in all cases. However, while directly calibrating the kinetic parameters would decrease reactivity in the fluidized bed, the good agreements found in the TGA experiments would be lost. To improve the comprehensive predictions, a more intricate modeling solution would require a competing high-temperature reaction path, including an initial step that is faster than the low-temperature mechanism, forming a solid intermediate, followed by slower decomposition kinetics that can predict the experiments in the fluidized bed. Since the focus of this paper is on comparing the models, not on improving them, no adjustment is

performed. For that step, experimental data from other reactors in the high-temperature range (e.g., drop tube or wire mesh reactors) must also be taken into account.

In contrast, the total volatile release rate can be predicted well with the Bio-CPD model. Good agreement with experimental data is achieved using the proposed parameter sets from Table 2, especially for cellulose and hemicellulose. It should be noted that these sets have been evaluated in a previous study [55] and were found to be the best combination of four available parameter sets [31,32,34,53] in the literature for each biomass component. For other parameter sets, similar or even higher deviations have been observed [55]. Notably, the parameter sets for lignin all overpredicted the release rates in a similar manner to the CRECK model, meaning that the fossil fuel-derived combination of structural and kinetic parameters [6,56] was identified as leading to the best model performance. One presumed reason for the good predictive accuracy of the Bio-CPD model is the use of experimental data from setups with high particle heating rates, so that flash pyrolysis conditions are achieved. The parameter set by Vizzini et al. [32] that was used for cellulose was calibrated against pure cellulose experiments performed by Scott et al. [25] in a fluidized bed reactor with particle heating rates in the range of 10^4–10^5 K s^{-1}. The set developed by Sheng and Azevedo [31] for hemicellulose was derived based on experimental data from a wire mesh reactor achieving particle heating rates of 10^3 K s^{-1}. Nevertheless, the use of biomass in which all three components are present at once might affect the determination of correct kinetic parameters. This fact might also be one of the reasons why the prediction of lignin conversion seems to be the most challenging problem as the contribution of lignin is tendentially the lowest compared to the other two fractions. Additionally, lignin shows the highest variety of structures and functional groups, making the origin of the extracted and separated lignin samples an influencing factor. Consequently, modeling and experimental investigation of lignin pyrolysis should be the focus of future research.

In general, the SFOR model is well suited describing the pyrolysis behavior in the fluidized bed reactor in terms of the total volatile release rates. A slightly better performance is obtained at higher temperatures and shorter reaction times and with simpler molecules (cellulose and hemicellulose). Thus, using the SFOR model to describe the pyrolysis process in CFD simulations with multiple other phenomena that have to be considered is an acceptable approach even bearing in mind the overall numerical effort in mind. Nevertheless, the user must be aware that certain characteristics of the pyrolysis process cannot be mapped. This can be seen, for example, in the final yields shown in Fig. 6. The SFOR model for lignin can approximately describe the release rate but underestimates the final yield since the contribution of very slow reactions in the SFOR model cannot be taken into account with the chosen calibration strategy.

4.3. Volatile yields in the fluidized bed reactor

Fig. 6 shows the final volatile yield split into a light gas and a tar fraction, wherever this differentiation is possible. The yield is obtained for an integration time of five times the time interval shown in Fig. 5, corresponding to $t = 375$ s for $T_{FB} = 673$ K, $t = 60$ s for $T_{FB} = 823$ K, and $t = 40$ s for $T_{FB} = 973$ K. The predictions from CRECK and Bio-CPD models that are shown here only reflect the output of primary pyrolysis reactions and do not include any effects of secondary gas-phase reactions. This topic will be discussed in Section 4.4.

Besides the volatiles release rates $\frac{dy_{vol}}{dt}$, the SFOR model is also able to predict the total volatile yield y_{vol}. This is unsurprising as the function for the final solid yield as a function of temperature $y_{s,\infty}(T)$ (compare Eq. (2)) is calibrated against the same experimental data. The deviation for lignin results from the fact that the SFOR model is fitted against the volatile release rate and thus is most sensitive to fast pyrolysis reactions. The products of the multiple slow reactions taking place in the lignin molecule are not taken into account in the fitting process. Different solutions to address this issue are discussed by Pielsticker et al. [39].

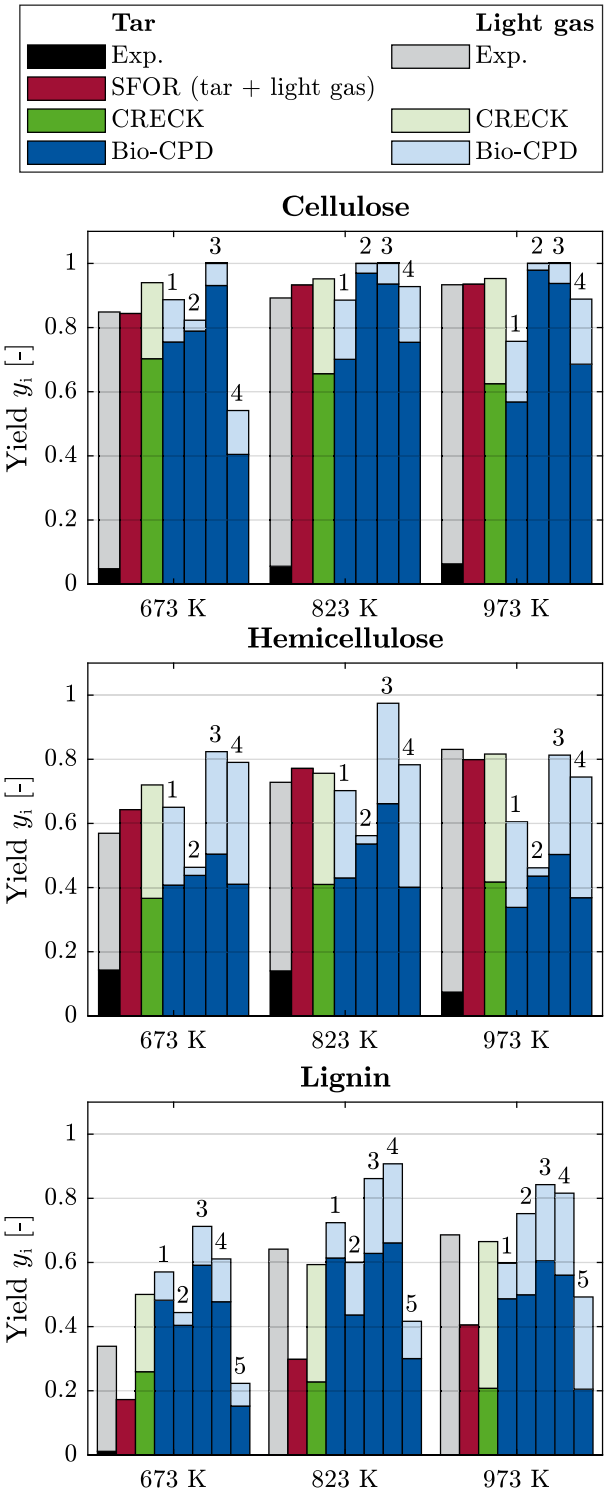

Fig. 6. Experimentally obtained total volatile yield separated into tar and light gas fractions in comparison with predictions from SFOR, CRECK, and Bio-CPD models at three different bed temperatures, not taking gas phase reactions into consideration. For the Bio-CPD model, predictions with different structure/kinetic parameter sets are given: (1) Sheng and Azevedo [31], (2) Vizzini et al. [32], (3) Lewis and Fletcher [34], (4) Wan et al. [53], and (5) Grant et al. [6] + Genetti et al. [56] (only for lignin).

Across all the biomass components and models, the CRECK model shows the closest prediction of temperature- and component-dependent total volatile yield compared to the experiments. Especially for the two higher temperatures T_{FB} = 823 K and T_{FB} = 973 K, the model predictions come very close to the experimental results (deviating by less than 7%). Only at the lower temperature T_{FB} = 673 K is the yield overestimated by 11 to 48% compared to the experimental results. Overall, the temperature sensitivity is less pronounced in the CRECK model than in the Bio-CPD model, which is in contrast to the observations of Rabaçal et al. [35].

The blue bars show the final yield predictions of the Bio-CPD model using all kinetic/structure parameter sets tested in the previous study [55], where the best-describing set was found via the comparison of the total volatile release rates. The shown rates from Fig. 5 correspond to parameter set (2) for cellulose, (1) for hemicellulose, and (5) for lignin in Fig. 6. Although the Bio-CPD model with these specific parameter sets makes the closest predictions of the volatile release rate (see Fig. 5) to the experiments, its predictions of the final volatile yield are more off than those of the other models. For cellulose and lignin, at least the temperature trend is shown correctly with the parameter sets (2) for cellulose and (5) for lignin, whereas the yield for hemicellulose decreases again for higher temperatures using the parameter set (2). However, this trend is also seen with all other parameter sets and not only for hemicellulose but also for cellulose and lignin, indicating a general improvement potential compared to the fossil-based parameter set (5), which captures the trend correctly. The wide range of predicted yields with the different parameter sets also presumably shows the strong dependence on the calibration data selected in each case.

Although the total yield of volatiles, or at least the trend, correlates well with the experimental results in many cases, the yield of tar is strongly overpredicted by all primary pyrolysis models. Consequently, secondary reactions in the gas phase must be present that convert parts of the tar into light gas. Thereby, the primary light gas yields given by the CRECK model are always higher than those from the Bio-CPD model.

4.4. Relevance of secondary reactions in the fluidized bed reactor

To evaluate the importance of secondary gas-phase reactions in the fluidized bed reactor, predictions employing and not employing different gas-phase reaction models are compared with one other and with the experimental data. Depending on the output of the primary pyrolysis model, the complexity of the usable gas-phase reaction models varies. While the CRECK model provides single gas species with known chemical formula and enables the use of the detailed gas-phase reaction mechanism CRECK-G-2003, the Bio-CPD model only gives the lumped species tar and light gas as output variables, meaning that only simplified tar cracking models can be used. As the SFOR model does not differentiate between any categories, it is not considered for secondary gas-phase reactions. The distribution of permanent light gases and condensable tar species is shown in Fig. 7.

When the CRECK primary pyrolysis model is combined with the CRECK-G-2003 secondary gas-phase reaction kinetics, almost no effect of secondary reactions is seen for the temperatures 673 and 823 K. Only at the bed temperature T_{FB} = 973 K does any significant decomposition of tar into light gases take place, and even then, it is far too low to reach the experimental results for all three fuels. A similar observation was already made for experiments using Columbian coal as a fuel [70]. To gain a deeper insight into the model output, the hatched areas show the tar fraction subdivided into different molecular sizes. The size classes are chosen based on the output of the Bio-CPD model in such a way that the fragment size consisting of N_{cl} = 1 clusters represents the reference unit, marked with the cross-hatched area. The hatched area above indicates smaller tar molecules, while the area below represents larger ones. For cellulose, this categorization is identical of using the monomer unit $C_6H_{10}O_5$ as a reference value.

With increasing temperature, for cellulose, the fraction of $C_6H_{10}O_5$ decreases, while the fraction of $C_6H_{10}O_5$ fragments (area with smaller molecular size) and primary light gas increases. While the CRECK model allows the monomer units to decompose further into small molecules, the Bio-CPD model requires the smallest tar fraction to be equal to the monomer unit and also does not allow the smallest fragment size to transition to the light gas fraction in the Bio-CPD model inside the particle. Consequently, the fraction of the $C_6H_{10}O_5$ fragment size increases as the temperature rises and decomposition progresses, while the light gas fraction stays comparably low. However, the predicted tars from the Bio-CPD include a large fraction of molecules with high molecular weight, which is not present in the predicted tars from the CRECK model. As all the fragments released to the gas phase are lumped as tar, it is impossible to further differentiate the different fragment sizes in the case of simulations with an active tar cracking model.

In the Bio-CPD model, the primary pyrolysis products from cellulose have the highest tar ratio of all the biomass components (95.8–97.8%). This comes on the one hand from the high linearity of the cellulose molecule, characterized by the low coordination number σ, and on the other hand from the low molecular weight m_{SC} of the side chains (16 u compared to 37 u for xylan and 58 u for lignin). While for cellulose and hemicellulose fragments with $N_{cl} > 1$ are present in significant amounts in the tar, the high molecular weight for lignin fragments hinders the transition from the liquid to the gaseous phase and thus the release from the particle.

Using the tar-cracking parameter set proposed by Fagbemi et al. [64], the tar yield is reduced by approximately 8 to 11%, but the temperature and residence time are too low to achieve a decomposition fraction similar to the experimental results. To achieve a light gas fraction of more than 80% in the volatiles, kinetic parameters as proposed by Pielsticker and Kneer [55] are required. While the activation energies in the two sets are almost identical, the pre-exponential factor is more than two orders of magnitude higher. The faster reaction may be provoked by the contact between the gases and hot solid particles in the bed [64,71].

Another reason might be the contribution of minerals included in the solid samples. Those minerals are either already present in the natural biomass or stem from the extraction process to gain the structural components [4]. The minerals have a catalytic effect, which may influence the reaction rates and the product spectrum depending on the ion concentration. Within the present study, only the CRECK model accounts for those catalytic effects. Thereby the activation energies of key reactions are adjusted based on the ash content (non-mineral specific). Low ash contents will higher the activation energy, while larger ones will lower it, whereby a saturation of the effect is assumed for ash contents higher than 4–5% [2]. For the Bio-CPD model, no implementation is considered in this study. However, Hameed et al. [19] recently tried to consider this effect for cellulose by changing the reaction kinetics of the bridge breaking (A_{lab}, $\mu_{E_{a,lab}}$, and $\sigma_{E_{a,lab}}$) and light gas formation (A_{LG}, $\mu_{E_{a,LG}}$, and $\sigma_{E_{a,LG}}$) depending on the loading of NaCl. However, the parameters have been obtained individually for each doping condition and no direct correlation with the NaCl mass fraction has been derived. Considering the catalytic effect of mineral components in the model leads to a decrease of tar by approximately 20 wt%, while light gas and char increase ≈10 wt% each. Within the study conducted by Ranzi et al. [72], the tar reduction during primary pyrolysis is approximately 10 wt%. Both studies highlight that the catalytic effect might be significant. However, the lack of detailed information on the mineral composition in the present samples and the current development status of the models prevent a more detailed consideration in this study but show clear development potential for further investigations.

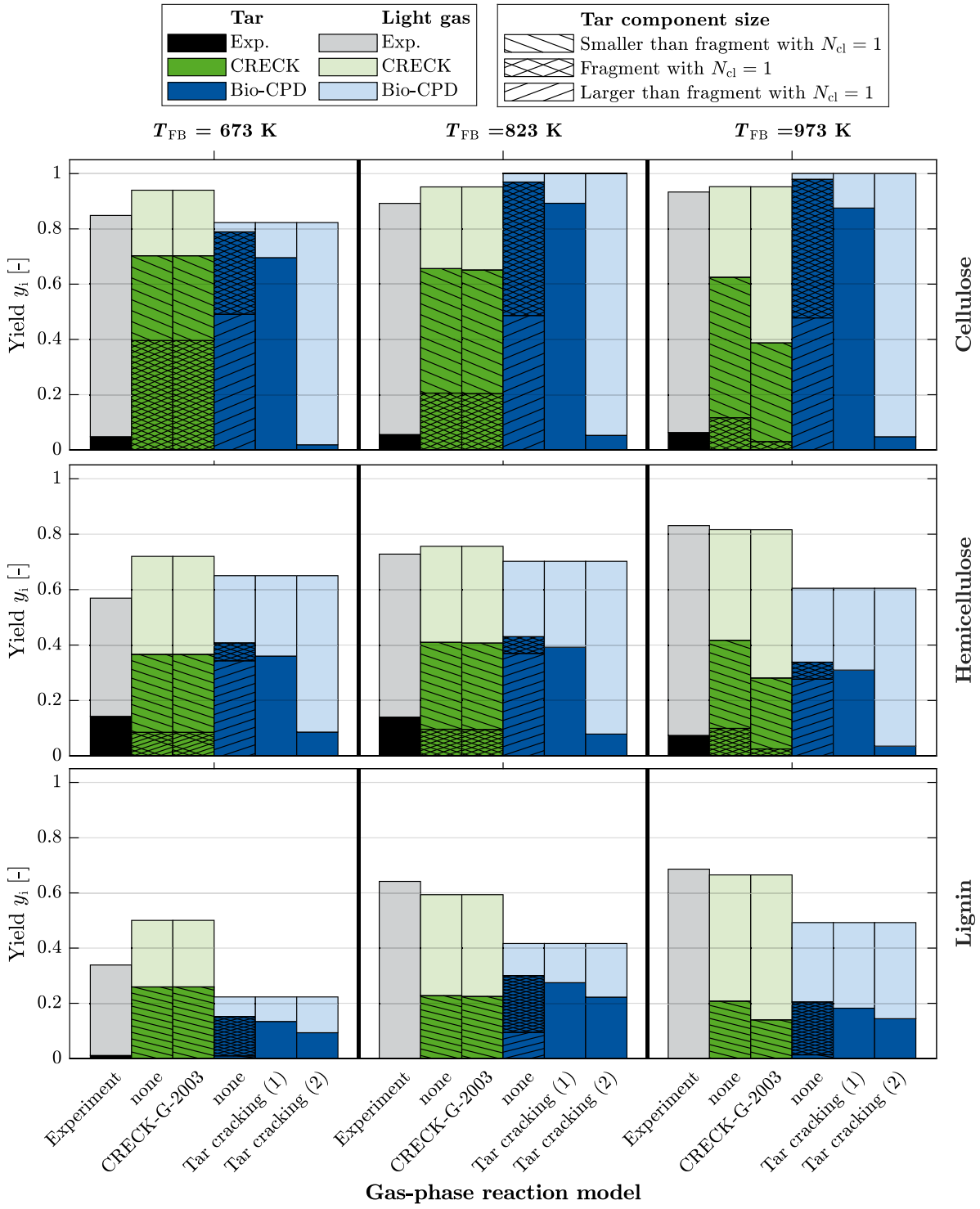

Fig. 7. Comparison of experimental light gas and tar yields obtained from pyrolysis in the FBR at three bed temperatures with model predictions using different secondary gas-phase reaction models (CRECK-G-2003 [22,65,66], first-order tar cracking model with either the parameter set from (1) Fagbemi [64] or (2) Pielsticker [55]). The hatched areas characterize the subdivision of the tar fraction into different molecular sizes, whereby the smallest fragment of the Bio-CPD model (N_{cl} = 1) serves as the reference. (For interpretation of the references to color in this figure legend, the reader is referred to the web version of this article.)

5. Conclusions

In the present study, a comprehensive analysis was undertaken regarding how three different pyrolysis models – namely the single first-order (SFOR), the chemical reaction engineering and chemical kinetics (CRECK), and the bio-based chemical percolation devolatilization (Bio-CPD) models – can predict the pyrolysis process of the extracted and separately pyrolyzed biomass components cellulose, hemicellulose (xylan) and lignin. Experimental reference data from thermogravimetric analysis and a small-scale fluidized bed reactor were used to evaluate the model performance under different thermal boundary conditions (low and high particle heating rate) regarding various output parameters, including the total volatile release rate, the total volatile yield, and the distribution of permanent light gases and condensable tar species.

One limiting factor for the SFOR model is that it cannot be considered fully predictive but always requires experimental data for calibration. In this study, the total volatile release rates in the FBR were chosen. In terms of its descriptive character, the SFOR model provides a better description when the molecule structure is simple (e.g., cellulose or hemicellulose) and the reactions mainly take place in parallel (fast heating in the FBR). Once the heating rate is lower and reactions become more sequential or the molecule structure becomes more complex (e.g., in lignin), the SFOR model is not capable of capturing the decomposition process correctly.

In contrast, the CRECK model predictions are closest to the experimental results regarding the decomposition in the TGA experiments, as the model includes several successive and parallel reactions whose reaction rates were determined using TGA experiments. Equally, the CRECK model was able to predict the total volatile yield under high heating rates at different bed temperatures for the three biomass components. However, the CRECK model tends to overestimate the release rate under flash pyrolysis conditions. Some reaction rates will most likely have to be recalibrated to suit experiments with high heating rates.

The peak of the total volatile release rate in the experiments is calculated with the smallest deviation from the Bio-CPD model. Its prediction of the total amount of volatiles released under flash pyrolysis conditions in the FBR also showed acceptable results in most cases. Potential for improvement was identified for the temperature dependency of the stabilization/side chain formation reaction for hemicellulose and, in general, for the lignin parameter set. In contrast, the Bio-CPD model was not able to correctly reflect the decomposition behavior in the TGA. This was mainly traced back to the fact that the CPD model, with its vapor–liquid equilibrium, originally stems from high-temperature flash pyrolysis performed with fossil fuels. These fuels have a molecular structure that consists of interconnected aromatic rings and thus differs strongly from the molecular structure of the biomass components, especially the polymers cellulose and hemicellulose, where the highest deviations are found.

The combination of primary pyrolysis models with secondary gas-phase reaction models allows a better comparison with the experimental results, obtained *ex situ* after a certain gas residence time in the bed and the pipe system. Neither the detailed CRECK-G-2003 mechanism nor the simplified tar cracking mechanism developed by Fagbemi et al. [64] predict the strong decomposition seen in the experimental results. It is only when the tar cracking reactivity is increased by two orders of magnitude that good accordance is found between the Bio-CPD prediction and experimental results, which may be explained by the hot surface of the bed material. The need for these high tar decomposition rates also results from the fact that the structure of the Bio-CPD model does not allow for decomposition extending further than the monomer unit, and thus only allows very small primary light gas contents compared to the CRECK model. Likewise, the catalytic effect of mineral components can lead to a significant reduction in the tar fraction and an increase in the light gas yield, requiring further investigation.

CRediT authorship contribution statement

Stefan Pielsticker: Writing – original draft, Investigation, Data curation, Conceptualization. **Paulo Debiagi:** Writing – review & editing, Investigation, Data curation. **Francesca Cerciello:** Writing – review & editing, Investigation, Conceptualization. **Christian Hasse:** Writing – review & editing, Project administration, Funding acquisition. **Reinhold Kneer:** Writing – review & editing, Supervision, Funding acquisition.

Declaration of competing interest

The authors declare the following financial interests/personal relationships which may be considered as potential competing interests: Stefan Pielsticker reports financial support was provided by German Research Foundation. Paulo Debiagi reports financial support was provided by German Research Foundation. If there are other authors, they declare that they have no known competing financial interests or personal relationships that could have appeared to influence the work reported in this paper.

Data availability

Dataset link: https://doi.org/10.18154/RWTH-2024-02457 and https://doi.org/10.18154/RWTH-2021-05544.

Acknowledgments

This work has been funded by the Deutsche Forschungsgemeinschaft (DFG, German Research Foundation) – 215035359 – SFB/TRR 129 ‘Oxyflame’.

References

[1] Debiagi P, Faravelli T, Hasse C, Ranzi E. Kinetic modeling of solid, liquid and gas biofuel formation from biomass pyrolysis. In: Production of biofuels and chemicals, vol. 10, Singapore: Springer Nature; 2020, p. 31–76. http://dx.doi.org/10.1007/978-981-15-2732-6_2.

[2] Ranzi E, Debiagi PEA, Frassoldati A. Mathematical modeling of fast biomass pyrolysis and bio-oil formation. Note I: Kinetic mechanism of biomass pyrolysis. ACS Sustain Chem Eng 2017;5(4):2867–81. http://dx.doi.org/10.1021/acssuschemeng.6b03096.

[3] Vikram S, Rosha P, Kumar S. Recent modeling approaches to biomass pyrolysis: A review. Energy Fuels 2021;35(9):7406–33. http://dx.doi.org/10.1021/acs.energyfuels.1c00251.

[4] Niksa S. On the primary devolatilization of hemicellulose. J Anal Appl Pyrolysis 2022;164:105515. http://dx.doi.org/10.1016/j.jaap.2022.105515.

[5] Hameed S, Sharma A, Pareek V, Wu H, Yu Y. A review on biomass pyrolysis models: Kinetic, network and mechanistic models. Biomass Bioenergy 2019;123:104–22. http://dx.doi.org/10.1016/j.biombioe.2019.02.008.

[6] Grant DM, Pugmire RJ, Fletcher TH, Kerstein AR. Chemical model of coal devolatilization using percolation lattice statistics. Energy Fuels 1989;3(2):175–86. http://dx.doi.org/10.1021/ef00014a011.

[7] Fletcher TH, Kerstein AR, Pugmire RJ, Grant DM. Chemical percolation model for devolatilization. 2. Temperature and heating rate effects on product yields. Energy Fuels 1990;4(1):54–60. http://dx.doi.org/10.1021/ef00019a010.

[8] Fletcher TH, Kerstein AR, Pugmire RJ, Solum MS, Grant DM. Chemical percolation model for devolatilization. 3. Direct use of ^{13}C NMR data to predict effects of coal type. Energy Fuels 1992;6(4):414–31. http://dx.doi.org/10.1021/ef00034a011.

[9] Solomon PR, Hamblen DG, Carangelo RM, Serio MA, Deshpande GV. General model of coal devolatilization. Energy Fuels 1988;2(4):405–22. http://dx.doi.org/10.1021/ef00010a006.

[10] Solomon PR, Hamblen DG, Serio MA, Yu Z-Z, Charpenay S. A characterization method and model for predicting coal conversion behaviour. Fuel 1993;72(4):469–88. http://dx.doi.org/10.1016/0016-2361(93)90106-C.

[11] Chen Y, Charpenay S, Jensen A, Wójtowicz MA, Serio MA. Modeling of biomass pyrolysis kinetics. Symp (Int) Combust 1998;27(1):1327–34. http://dx.doi.org/10.1016/S0082-0784(98)80537-7.

[12] Niksa S, Kerstein AR. Flashchain theory for rapid coal devolatilization kinetics. 1. Formulation. Energy Fuels 1991;5(5):647–65. http://dx.doi.org/10.1021/ef00029a006.

[13] Niksa S. Flashchain theory for rapid coal devolatilization kinetics. 2. Impact of operating conditions. Energy Fuels 1991;5(5):665–73. http://dx.doi.org/10.1021/ef00029a007.

[14] Niksa S. Flashchain theory for rapid coal devolatilization kinetics. 3. Modeling the behavior of various coals. Energy Fuels 1991;5(5):673–83. http://dx.doi.org/10.1021/ef00029a008.

[15] Niksa S. Predicting the rapid devolatilization of diverse forms of biomass with bio-flashchain. Proc Combust Inst 2000;28(2):2727–33. http://dx.doi.org/10.1016/S0082-0784(00)80693-1.

[16] Yan B-H, Cheng Y, Xu P, Cao C-X, Cheng Y. Generalized model of heat transfer and volatiles evolution inside particles for coal devolatilization. AIChE J 2014;60(8):2893–906. http://dx.doi.org/10.1002/aic.14484.

[17] de Girolamo A, Tan V, Liu Z, Zhang L. Pyrolysis of a lignite briquette – Experimental investigation and 1-dimensional modelling approach. Fuel 2018;212:533–45. http://dx.doi.org/10.1016/j.fuel.2017.10.021.

[18] Ma J, Liu J, Jiang X, Chen B. Improved CPD model coupled with lattice vacancy evolution. Combust Flame 2022;241:112076. http://dx.doi.org/10.1016/j.combustflame.2022.112076.

[19] Hameed S, Wagh AS, Sharma A, Pareek V, Yu Y, Joshi JB. Kinetic modelling of pyrolysis of cellulose using CPD model: Effect of salt. J Therm Anal Calorim 2022;147(17):9763–77. http://dx.doi.org/10.1007/s10973-021-11192-5.

[20] Papari S, Hawboldt K. A review on the pyrolysis of woody biomass to bio-oil: Focus on kinetic models. Renew Sustain Energy Rev 2015;52:1580–95. http://dx.doi.org/10.1016/j.rser.2015.07.191.

[21] Anca-Couce A, Mehrabian R, Scharler R, Obernberger I. Kinetic scheme of biomass pyrolysis considering secondary charring reactions. Energy Convers Manag 2014;87:687–96. http://dx.doi.org/10.1016/j.enconman.2014.07.061.

[22] Ranzi E, Frassoldati A, Stagni A, Pelucchi M, Cuoci A, Faravelli T. Reduced kinetic schemes of complex reaction systems: Fossil and biomass-derived transportation fuels. Int J Chem Kinet 2014;46(9):512–42. http://dx.doi.org/10.1002/kin.20867.

[23] Ranzi E, Cuoci A, Faravelli T, Frassoldati A, Migliavacca G, Pierucci S, Sommariva S. Chemical kinetics of biomass pyrolysis. Energy Fuels 2008;22(6):4292–300. http://dx.doi.org/10.1021/ef800551t.

[24] Debiagi P, Gentile G, Cuoci A, Frassoldati A, Ranzi E, Faravelli T. A predictive model of biochar formation and characterization. J Anal Appl Pyrolysis 2018;134:326–35. http://dx.doi.org/10.1016/j.jaap.2018.06.022.

[25] Scott DS, Piskorz J, Bergougnou MA, Graham R, Overend RP. The role of temperature in the fast pyrolysis of cellulose and wood. Ind Eng Chem Res 1988;27(1):8–15. http://dx.doi.org/10.1021/ie00073a003.

[26] Nunn TR, Howard JB, Longwell JP, Peters WA. Product compositions and kinetics in the rapid pyrolysis of sweet gum hardwood. Ind Eng Chem Process Des Dev 1985;24(3):836–44. http://dx.doi.org/10.1021/i200030a053.

[27] Wagenaar BM, Prins W, van Swaaij WPM. Flash pyrolysis kinetics of pine wood. Fuel Process Technol 1993;36(1–3):291–8. http://dx.doi.org/10.1016/0378-3820(93)90039-7.

[28] Sun S, Tian H, Zhao Y, Sun R, Zhou H. Experimental and numerical study of biomass flash pyrolysis in an entrained flow reactor. Bioresour Technol 2010;101(10):3678–84. http://dx.doi.org/10.1016/j.biortech.2009.12.092.

[29] Septien S, Valin S, Dupont C, Peyrot M, Salvador S. Effect of particle size and temperature on woody biomass fast pyrolysis at high temperature (1000–1400 °C). Fuel 2012;97:202–10. http://dx.doi.org/10.1016/j.fuel.2012.01.049.

[30] Fraga A-R, Gaines AF, Kandiyoti R. Characterization of biomass pyrolysis tars produced in the relative absence of extraparticle secondary reactions. Fuel 1991;70(7):803–9. http://dx.doi.org/10.1016/0016-2361(91)90186-E.

[31] Sheng C, Azevedo JLT. Modeling biomass devolatilization using the chemical percolation devolatilization model for the main components. Proc Combust Inst 2002;29(1):407–14. http://dx.doi.org/10.1016/S1540-7489(02)80054-2.

[32] Vizzini G, Bardi A, Biagini E, Falcitelli M, Tognotti L. Prediction of rapid biomass devolatilization yields with an upgraded version of the bio-CPD model. In: 31st meeting of the Italian section of the combustion institute. 2008.

[33] Fletcher TH, Pond HR, Webster J, Wooters J, Baxter LL. Prediction of tar and light gas during pyrolysis of black liquor and biomass. Energy Fuels 2012;26(6):3381–7. http://dx.doi.org/10.1021/ef300574n.

[34] Lewis AD, Fletcher TH. Prediction of sawdust pyrolysis yields from a flat-flame burner using the CPD model. Energy Fuels 2013;27(2):942–53. http://dx.doi.org/10.1021/ef3018783.

[35] Rabaçal M, Costa M, Vascellari M, Hasse C. Kinetic modelling of sawdust and beech wood pyrolysis in drop tube reactors using advanced predictive models. Chem Eng Trans 2014;37:79–84. http://dx.doi.org/10.3303/CET1437014.

[36] Maffei T, Senneca O, Ranzi E, Salatino P. Pyrolysis, annealing and char combustion/oxy-combustion for CFD codes. In: 34th meeting of the Italian section of the combustion institute. 2011.

[37] Richards AP, Fletcher TH. A comparison of simple global kinetic models for coal devolatilization with the CPD model. Fuel 2016;185:171–80. http://dx.doi.org/10.1016/j.fuel.2016.07.095.

[38] Xing J, Kurose R, Luo K, Fan J. Chemical reaction neural network modelling of lignocellulosic biomass pyrolysis. SSRN Electron J 2023. http://dx.doi.org/10.2139/ssrn.4342806.

[39] Pielsticker S, Gövert B, Umeki K, Kneer R. Flash pyrolysis kinetics of extracted lignocellulosic biomass components. Front Energy Res 2021;9. http://dx.doi.org/10.3389/fenrg.2021.737011.

[40] Ranzi E, Corbetta M, Manenti F, Pierucci S. Kinetic modeling of the thermal degradation and combustion of biomass. Chem Eng Sci 2014;110:2–12. http://dx.doi.org/10.1016/j.ces.2013.08.014.

[41] Gao X, Lu L, Shahnam M, Rogers WA, Smith K, Gaston K, Robichaud D, Brennan Pecha M, Crowley M, Ciesielski PN, Debiagi P, Faravelli T, Wiggins G, Finney CE, Parks JE. Assessment of a detailed biomass pyrolysis kinetic scheme in multiscale simulations of a single-particle pyrolyzer and a pilot-scale entrained flow pyrolyzer. Chem Eng J 2021;418:129347. http://dx.doi.org/10.1016/j.cej.2021.129347.

[42] Houston R, Oyedeji O, Abdoulmoumine N. Detailed biomass fast pyrolysis kinetics integrated to computational fluid dynamic (CFD) and discrete element modeling framework: Predicting product yields at the bench-scale. Chem Eng J 2022;444:136419. http://dx.doi.org/10.1016/j.cej.2022.136419.

[43] Sánchez M, Maya JC, Pecha B, Chejne F, Quinchía-Figueroa AM. Effect of particle characteristics, kinetics and transport phenomena on the prediction of particle mass loss and products yields during biomass fast pyrolysis. J Anal Appl Pyrolysis 2022;168:105786. http://dx.doi.org/10.1016/j.jaap.2022.105786.

[44] Berkel L, Debiagi P, Nicolai H, Amjed MA, Stagni A, Hasse C, Faravelli T. Development of a multiphase chemical reactor network method as a tool for simulating biomass gasification in fluidized beds. Fuel 2024;357:129731. http://dx.doi.org/10.1016/j.fuel.2023.129731.

[45] Pielsticker S, Schlögel KU, Kreitzberg T, Hatzfeld O, Kneer R. Biomass pyrolysis kinetics in a fluidized bed reactor: Measurements and plausibility verification for reaction conditions. Fuel 2019;254:115589. http://dx.doi.org/10.1016/j.fuel.2019.05.172.

[46] Pielsticker S, Gövert B, Kreitzberg T, Habermehl M, Hatzfeld O, Kneer R. Development of a rapidly responding fluidized bed reactor by theoretical and experimental evaluation of combustion reactions. Fuel 2018;223:462–9. http://dx.doi.org/10.1016/j.fuel.2018.02.171.

[47] Pielsticker S, Gövert B, Umeki K, Kneer R. Flash pyrolysis kinetics of extracted lignocellulosic biomass components – Supplementary dataset. 2021, http://dx.doi.org/10.18154/RWTH-2021-05544.

[48] Al-Abbas AH, Naser J, Dodds D. CFD modelling of air-fired and oxy-fuel combustion of lignite in a 100 kW furnace. Fuel 2011;90(5):1778–95. http://dx.doi.org/10.1016/j.fuel.2011.01.014.

[49] Chen L, Ghoniem AF. Simulation of oxy-coal combustion in a 100 kw_{th} test facility using RANS and LES: A validation study. Energy Fuels 2012;26(8):4783–98. http://dx.doi.org/10.1021/ef3006993.

[50] Franchetti BM, Cavallo Marincola F, Navarro-Martinez S, Kempf AM. Large eddy simulation of a 100 kw_{th} swirling oxy-coal furnace. Fuel 2016;181:491–502. http://dx.doi.org/10.1016/j.fuel.2016.05.015.

[51] Nicolai H, Wen X, Miranda FC, Zabrodiec D, Maß meyer A, di Mare F, Dreizler A, Hasse C, Kneer R, Janicka J. Numerical investigation of swirl-stabilized pulverized coal flames in air and oxy-fuel atmospheres by means of large eddy simulation coupled with tabulated chemistry. Fuel 2020;119429. http://dx.doi.org/10.1016/j.fuel.2020.119429.

[52] Ku X, Shen F, Jin H, Lin J, Li H. Simulation of biomass pyrolysis in a fluidized bed reactor using thermally thick treatment. Ind Eng Chem Res 2019;58(4):1720–31. http://dx.doi.org/10.1021/acs.iecr.8b04778.

[53] Wan K, Wang Z, He Y, Xia J, Zhou Z, Zhou J, Cen K. Experimental and modeling study of pyrolysis of coal, biomass and blended coal-biomass particles. Fuel 2015;139:356–64. http://dx.doi.org/10.1016/j.fuel.2014.08.069.

[54] Pielsticker S, Ontyd C, Kreitzberg T, Hatzfeld O, Schiemann M, Scherer V, Kneer R. Adaptation of the chemical percolation devolatilization model for low temperature pyrolysis in a fluidized bed reactor. Combust Sci Technol 2019;52:1–18. http://dx.doi.org/10.1080/00102202.2019.1682433.

[55] Pielsticker S, Kneer R. Modeling pyrolysis kinetics of extracted biomass components with the bio-chemical percolation devolatilization model. Fuel 2024;360:130454. http://dx.doi.org/10.1016/j.fuel.2023.130454.

[56] Genetti D, Fletcher TH, Pugmire RJ. Development and application of a correlation of ^{13}C NMR chemical structural analyses of coal based on elemental composition and volatile matter content. Energy Fuels 1999;13(1):60–8. http://dx.doi.org/10.1021/ef980074k.

[57] Fisher ME, Essam JW. Some cluster size and percolation problems. J Math Phys 1961;2(4):609–19. http://dx.doi.org/10.1063/1.1703745.

[58] King CJ. Separation processes. McGraw-hill chemical engineering series, 2nd ed.. New York: McGraw-Hill; 1980.

[59] Fang Z, Smith RL, Xu L, editors. Production of biofuels and chemicals. Singapore: Springer; 2020.

[60] Merrick D. Mathematical models of the thermal decomposition of coal. Fuel 1983;62(5):534–9. http://dx.doi.org/10.1016/0016-2361(83)90222-3.

[61] Gunn DJ. Transfer of heat or mass to particles in fixed and fluidised beds. Int J Heat Mass Transfer 1978;21(4):467–76. http://dx.doi.org/10.1016/0017-9310(78)90080-7.

[62] Lienhard I.V. JH, Lienhard V. JH. A heat transfer textbook. 3rd ed.. Cambridge, Massachusetts (USA): Phlogiston Press; 2008.

[63] Branca C, Di Blasi C. A summative model for the pyrolysis reaction heats of beech wood. Thermochim Acta 2016;638:10–6. http://dx.doi.org/10.1016/j.tca.2016.06.006.

[64] Fagbemi L, Khezami L, Capart R. Pyrolysis products from different biomasses. Appl Energy 2001;69(4):293–306. http://dx.doi.org/10.1016/S0306-2619(01)00013-7.

[65] Ranzi E, Cavallotti C, Cuoci A, Frassoldati A, Pelucchi M, Faravelli T. New reaction classes in the kinetic modeling of low temperature oxidation of n-alkanes. Combust Flame 2015;162(5):1679–91. http://dx.doi.org/10.1016/j.combustflame.2014.11.030.

[66] Bagheri G, Ranzi E, Pelucchi M, Parente A, Frassoldati A, Faravelli T. Comprehensive kinetic study of combustion technologies for low environmental impact: MILD and oxy-fuel combustion of methane. Combust Flame 2020;212:142–55. http://dx.doi.org/10.1016/j.combustflame.2019.10.014.

[67] Abad A, Cardona SC, Torregrosa JI, López F, Navarro-Laboulais J. Flow analysis deconvolution for kinetic information reconstruction. J Math Chem 2005;38(2):271–92. http://dx.doi.org/10.1007/s10910-005-5422-8.

[68] Pielsticker S, Debiagi P, Cerciello F, Hasse C, Kneer R. Comparative analysis of pyrolysis models including SFOR, CRECK, and bio-CPD to predict reaction kinetics and products from extracted biomass components – Supplementary dataset. 2024, http://dx.doi.org/10.18154/RWTH-2024-02457.

[69] Piskorz J, Radlein D, Scott DS. On the mechanism of the rapid pyrolysis of cellulose. J Anal Appl Pyrolysis 1986;9(2):121–37. http://dx.doi.org/10.1016/0165-2370(86)85003-3.

[70] Debiagi P, Ontyd C, Pielsticker S, Schiemann M, Faravelli T, Kneer R, Hasse C, Scherer V. Calibration and validation of a comprehensive kinetic model of coal conversion in inert, air and oxy-fuel conditions using data from multiple test rigs. Fuel 2020;119682. http://dx.doi.org/10.1016/j.fuel.2020.119682.

[71] Liden AG, Berruti F, Scott DS. A kinetic model for the production of liquids from the flash pyrolysis of biomass. Chem Eng Commun 1988;65(1):207–21. http://dx.doi.org/10.1080/00986448808940254.

[72] Ranzi E, Debiagi P, Frassoldati A. Mathematical modeling of fast biomass pyrolysis and bio-oil formation. Note II: Secondary gas-phase reactions and bio-oil formation. ACS Sustain Chem Eng 2017;5(4):2882–96. http://dx.doi.org/10.1021/acssuschemeng.6b03098.